Quantum doubles in symmetric blockade structures

Hans Peter Büchler,[*,†] Tobias F. Maier,[†] Simon Fell,[†] and Nicolai Lang[†]
Institute for Theoretical Physics III and Center for Integrated Quantum Science and Technology, University of Stuttgart, 70550 Stuttgart, Germany

(Received 6 November 2025; revised 11 June 2026; accepted 12 June 2026; published 9 July 2026)

Exactly solvable models of topologically ordered phases with non-Abelian anyons typically require complicated many-body interactions that do not arise naturally. This motivates the "inverse problem" of quantum many-body physics: How to design a microscopic Hamiltonian that realizes a desired topological phase with a given, restricted type of two-body interactions? Here, we address this problem for systems where elementary two-level degrees of freedom couple via simple blockade interactions, a platform motivated by Rydberg atoms. Within this framework, we construct Hamiltonians that realize topological orders described by non-Abelian quantum double models. We analytically prove the existence of topological order in the ground states and present efficient schemes to prepare these states. We also introduce protocols for the controlled adiabatic braiding of anyonic excitations that probe their non-Abelian statistics. Our construction is generic and applies to quantum doubles $\mathcal{D}(G)$ for arbitrary finite groups G. We illustrate braiding for the simplest non-Abelian quantum double $\mathcal{D}(S_3)$.

DOI: 10.1103/99sy-kggw

I. INTRODUCTION

The ground-state phase diagrams of quantum many-body systems at zero temperature can be extremely rich. Of special interest are quantum phases with properties that are unique to quantum systems. One of the most intriguing examples are topologically ordered phases of two-dimensional systems that are characterized by their pattern of long-range entanglement [1–4]. It is the entanglement structure of these gapped ground states that entails anyonic statistics of excitations and robust ground-state degeneracies on topologically nontrivial manifolds. While topological phases with Abelian anyonic excitations have useful applications as quantum error correction codes [5–7], phases with non-Abelian excitations are of special interest because of their higher-dimensional braid group representations, making them potential substrates for topological quantum computing [8–10]. While there is general consensus that some fractional quantum Hall states are natural examples of topological orders with Abelian anyons [11,12], the realization of non-Abelian phases in fractional quantum Hall states or artificial matter is much more challenging [9,13,14]. Especially the experimental detection of their characteristic entanglement structure (e.g., by probing the anyonic braiding statistics) is still an open problem. Meanwhile, on the theory side, there are thoroughly explored models that give rise to a large variety of topological orders with non-Abelian anyons. Examples are Chern–Simons theories for fractional quantum Hall states [15–17], Kitaev's quantum double models [5], and string-net condensates [18,19], as well as other minimalistic models [20,21]. Unfortunately, most of these models rely on nontrivial multibody interactions that do not naturally occur—a major roadblock for experimentally exploring these topological orders. This motivates the "inverse problem" of quantum many-body physics: Given a microscopic platform with a particular type of two-body interactions and tunability of elementary degrees of freedom, is it possible—and if so how—to engineer quantum systems that realize interesting quantum many-body ground states? In this paper, we consider systems characterized by two-body blockade interactions and show how these can be used to systematically engineer microscopic models that realize a large class of non-Abelian topological orders.

In recent years, a major goal has been to realize and probe topological phases in artificial matter. In condensed-matter settings, p-wave superconductors are promising for the realization of Majorana zero modes, either on the boundaries of wires [22,23] or in the core of vortices [24,25], while recent progress with two-dimensional van der Waals materials opens a pathway towards fractional Chern insulators [26–29]. The framework of quantum simulation provides another promising approach, where a variety of systems based on cold atomic and molecular gases have been put forward. First theoretical proposals focused on the realization of Kitaev's honeycomb model [20] in optical lattices [30] or using a spin toolbox realized by polar molecules [31]. Other proposals target the realization of fractional quantum Hall states with rotating gases [32], Majorana modes in double wires [33] and p-wave superfluids [34], and bosonic fractional Chern insulators with polar molecules [35] and Rydberg atoms [36]. Focusing on superconducting circuits, artificial spin models with competing

[*]Contact author: hans-peter.buechler@itp3.uni-stuttgart.de
[†]These authors contributed equally to this work.

ferromagnetic and antiferromagnetic two-body interactions have been proposed [37–41]. These feature local, microscopic symmetries (so-called "combinatorial gauge symmetries"), and perturbative arguments suggest that they can stabilize abelian and non-Abelian topological orders. In recent years, especially Rydberg atoms have emerged as a promising platform to study topological phases, with the first experimental observation of a symmetry-protected topological phase in one dimension [42], and attempts to probe a $\mathbb{Z}_2$ spin liquid with toric code topological order [43,44]. (The experimentally observed signatures are, however, most likely a consequence of dynamical state preparation, rather than ground-state properties of the engineered Hamiltonian [45,46].) The advantage of the Rydberg platform is the high flexibility to arrange atoms in arbitrary two- [47–49] and three-dimensional geometries [50], local optical access to individual atoms, a large freedom to select internal states to engineer microscopic Hamiltonians, as well as strong van der Waals and dipolar exchange interactions between different Rydberg levels [51–53]. Notably, the strong van der Waals coupling can often be modeled by a simple blockade interaction [49,54–60]: A strong (infinite) interaction on distances shorter than a tunable blockade radius, and a vanishing interaction on larger distances. The simplicity of this coupling makes Rydberg atoms a versatile platform for the bottom-up design of artificial quantum matter.

In the first part of this paper, we use a framework inspired by the Rydberg platform to design microscopic Hamiltonians with ground states that are in the topological phase of Kitaev's paradigmatic quantum double models (of which the toric code is the simplest example [5]). The latter are characterized by a finite group G and, for non-Abelian groups, their topological order supports non-Abelian anyonic excitations. Our framework is based on microscopic two-level systems, arranged in a periodic two-dimensional structure, with local detunings, local transverse fields, and simple two-body blockade interactions. The approach presented here is the natural extension to arbitrary groups G of the construction described in Ref. [61] for the abelian group $\mathbb{Z}_2$. The main idea is that blockade interactions can be abstractly described by vertex-weighted *blockade graphs*, and the design of these graphs can be guided by two crucial insights. First, ground states map to *maximum-weight independent sets* and satisfy local constraints that are encoded in the topology of these graphs. Second, blockade graphs can feature *local graph automorphisms* that translate to local unitary symmetries of the Hamiltonian, which, in turn, enforce strong quantum fluctuations within the subspace of states that satisfy the local constraints. While closely related models with local symmetries have been recently proposed [37–41], the Hamiltonians introduced here can be constructed graphically, are more natural for the Rydberg platform, and, most importantly, allow for a rigorous proof that their ground state is in the topological phase of the prescribed quantum double $\mathcal{D}(G)$ for weak transverse fields. Furthermore, a spectral gap to flux anyons can be proved in the thermodynamic limit. A finite *charge* gap is expected as well, but much more challenging to show rigorously; a proof for the special case $G = \mathbb{Z}_2$ is in preparation [62].

In the second part of the paper, we leverage our framework to propose an efficient scheme for adiabatically preparing these ground states, together with a controllable procedure to prepare states with localized anyons. Finally, we propose an efficient protocol for the adiabatic braiding of anyons to probe their non-Abelian statistics. While our construction is generic and works for arbitrary groups G, we illustrate the braiding protocol for the simplest non-Abelian quantum double $\mathcal{D}(S_3)$.

We emphasize that all results in the first part of the paper are backed by mathematically rigorous proofs that remain valid in the presence of weak but finite transverse fields. By contrast, the results in the second part are only rigorous within the symmetry sectors of these models. Finally, we note that, while being inspired by the Rydberg platform, all constructions in this paper are platform-agnostic and allow for alternative realizations, e.g., with polar molecules in optical tweezers [63] or superconducting qubits connected by microwave cavities acting as a bus to mediate blockade interactions [64].

II. THE MODEL

A. Review: Blockade structures

We consider extensive *blockade structures* $\mathcal{G}$ of two-level systems arranged in space. We denote the total Hilbert space of such a structure by $\mathcal{H}_\mathcal{G}$. The two-level systems i are subject to a uniform transverse field Ω and local detunings Δ_i, and interact via an isotropic blockade potential [49,54–60]; i.e., their interaction vanishes at large distances and saturates at a value U_0 on distances shorter than a blockade radius r_B,

$$U(r) := \begin{cases} 0 & \text{for } r > r_\mathrm{B}, \\ U_0 & \text{for } r \leqslant r_\mathrm{B}. \end{cases} \tag{1}$$

Note that in the context of blockade interactions, U_0 is often set to infinity. Here, we keep it as a free but large, positive parameter, which has no effect on our results but makes rigorous statements easier to prove. The simplicity of the blockade potential (1) suggests encoding the spatial arrangement of a structure $\mathcal{G}$ by a *vertex-weighted blockade graph* $\mathcal{G} \equiv (V, E, W)$: The two-level systems $i \in V$ form the *vertices* V of the graph, so that the Hilbert space of the structure has the form $\mathcal{H}_\mathcal{G} = (\mathbb{C}^2)^{\otimes |V|}$. The detunings are interpreted as the *weights* $W \equiv \{\Delta_i\}$ of the vertices, and the *edges* $e = \{i, j\} \in E$ of the graph denote pairs of two-level systems that are in blockade (i.e., are separated by less than the blockade radius r_B).

With these conventions, the Hamiltonian associated with a blockade structure (or *blockade graph*) $\mathcal{G}$ has the form

$$H_\mathcal{G} = H^0_\mathcal{G} + \Omega \sum_{i \in V} \sigma^x_i$$
$$\text{with} \quad H^0_\mathcal{G} = U_0 \sum_{\{i,j\} \in E} n_i n_j - \sum_{i \in V} \Delta_i n_i, \tag{2}$$

where σ^α_i denotes the Pauli matrices for each two-level system and $n_i = (1 - \sigma^z_i)/2$ is the projector onto the state $|1\rangle_i$. The summation of the interaction term in (2) runs over all pairs $\{i, j\} \in E$ of vertices that are connected by an edge of the blockade graph $\mathcal{G}$. Clearly, there exists a one-to-one correspondence between Hamiltonians of the form (2) and vertex-weighted graphs $\mathcal{G}$ for every transverse field Ω. However, note that not every abstract graph can be realized as the blockade graph of a spatial structure in two

or three dimensions. The Hamiltonian (2) belongs to the class of transverse-field Ising models in the presence of a site-dependent longitudinal field Δ_i. The complexity and versatility of this family of Hamiltonians (e.g., to realize non-Abelian topological phases) are hidden in the spatial arrangement of the two-level systems, and therefore the choice of which pairs of two-level systems are in blockade:

For $\Omega = 0$, the ground-state manifold becomes classical and is characterized by the frustration between detuning and blockade interactions. With $\Delta_i > 0$, the energy can be lowered by exciting two-level systems, while the blockade interaction $U_0 \gg \Delta_i$ penalizes most patterns with many excitations. The ground-state manifold is then spanned by product states with excitation patterns that form *maximum-weight independent sets* of the blockade graph $\mathcal{G}$ [54]; finding these patterns for a given blockade graph is a known **NP**-hard problem [65,66]. Some of us have shown previously how this complexity can be leveraged for the systematic construction of (classical) blockade Hamiltonians in two dimensions that enforce arbitrary local constraints on excitation patterns in the ground-state manifold [60], a feature that can be used, for example, to implement local Gauss laws. This result is built on two core insights: First, blockade Hamiltonians allow for the implementation of elementary Boolean constraints in their classical ground-state manifold, in particular the universal NOR-gate (Not-OR). Second, these primitives can be combined via a construction called *amalgamation,* in which certain two-level systems are identified and their detunings are added. In combination, these features allow for the implementation of arbitrary Boolean circuits as blockade Hamiltonians with ground-state manifolds spanned by excitation patterns that satisfy the Boolean circuit. In Ref. [60] we demonstrated how this universality can be used to engineer blockade structures that enforce the local loop constraints that characterize the $\mathcal{D}(\mathbb{Z}_2)$ topological order of the paradigmatic toric code [5,67]; in the present paper, we generalize this construction to the non-Abelian constraints needed for generic quantum doubles $\mathcal{D}(G)$ (Secs. II B and II C).

For $\Omega \neq 0$, the quantum fluctuations in (2) stabilize an unknown superposition of the classically engineered excitation patterns as quantum many-body ground states. Since, for generic blockade graphs, (2) cannot be diagonalized exactly, the characterization of its ground-state manifold is typically restricted to perturbative and numerical methods. However, in the follow-up Ref. [61], some of us identified a class of symmetries that allows for the construction of special blockade Hamiltonians with rigorous control over the quantum fluctuations in the ground-state manifold. Notably, these systems are *not* renormalization fixed points and cannot be diagonalized exactly. Nonetheless, a rigorous characterization of the long-range entanglement in their ground state is possible, and the existence of spectral bulk gaps within symmetry sectors can be proved. The underlying symmetries are *blockade graph automorphisms*, i.e., permutations of the vertices of $\mathcal{G}$ such that the graph remains unchanged (if edges are allowed to "pass through each other"). These automorphisms induce a unitary action on the classical ground-state manifold (permuting vertices/two-level systems permutes excitations). If the classical ground-state manifold of a blockade Hamiltonian has the special feature that all ground-state excitation patterns can be transformed into each other by such permutations, we call the blockade structure *fully symmetric*. The core insight is that full symmetry enforces *equal-weight superpositions* of the classical excitation patterns in the ground state once quantum fluctuations are switched on ($\Omega \neq 0$). In Ref. [61] we exploited this feature to realize the abelian topological order $\mathcal{D}(\mathbb{Z}_2)$ of the toric code; in the present paper, we show how full symmetry can be leveraged to realize more general quantum double topological orders $\mathcal{D}(G)$ (Sec. III). In contrast to the toric code, these models can host *non-Abelian* topological orders. Hence, the more general construction in this paper sets the stage for exploring non-Abelian braiding and fusion of anyonic excitations in a microscopic setting with only two-body interactions (Secs. IV and V); we discuss this in detail for the non-Abelian group $G = S_3$ (Sec. VI).

B. Review: Quantum doubles

Our goal is the generic construction of a family of blockade graphs $\mathcal{G}$ such that the ground states of the corresponding Hamiltonians (2) realize all topological phases of Kitaev's *quantum double models* [5,67–71], defined on a honeycomb lattice with trivalent sites (Fig. 1). These models are derived from a finite group G of order $N = |G|$. To each element $g \in G$ a quantum state $|g\rangle$ is assigned on every *link* of the lattice; thus the Hilbert space of the quantum double on a periodic honeycomb lattice with A unit cells is $\mathcal{H}_G = (\mathbb{C}^N)^{\otimes 3A}$. In addition, we assign an orientation to each link; it is convenient to choose all links incoming (outgoing) on alternating lattice sites, see Fig. 1(a). Then, the Hamiltonian of the quantum double model can be written as

$$H_G = -J_s \sum_{\text{Sites } s} B_s - J_p \sum_{\text{Faces } p} \underbrace{\frac{1}{N} \sum_{h \in G} A_p(h)}_{A_p} \tag{3}$$

with $J_s > 0$ and $J_p > 0$. (Note that we are using the convention of Simon [67]—which is formulated on the *dual* lattice of the original model introduced by Kitaev [5].)

The *site operators* B_s are local projectors onto configurations where the three states $|g_1\rangle$, $|g_2\rangle$ and $|g_3\rangle$ on the links adjacent to site s obey the "no-flux" constraint $g_1 g_2 g_3 = \mathrm{e}$ with $\mathrm{e} \in G$ the identity of the group G. Note that in general the group G is non-Abelian and therefore the order of multiplication is important; here we follow the convention with clockwise multiplication on sites with outward-pointing arrows, and counterclockwise multiplication on sites with inward-pointing arrows [Fig. 1(a)]. The *plaquette operators* $A_p(h)$ flip between such configurations by changing each state $|g_l\rangle$ on links $l \in p$ bounding plaquette p to $|hg_l\rangle$ or $|g_l h^{-1}\rangle$: if the arrow on the link is parallel to the counterclockwise orientation of the loop surrounding the plaquette, the action is $|hg_l\rangle$ on this link (= the plaquette is on the left of the link arrow); otherwise, the action is $|g_l h^{-1}\rangle$ (= the plaquette is on the right of the link arrow), see Fig. 1(a). The sum A_p of $A_p(h)$ over all group elements $h \in G$ defined in Eq. (3) is then again a projector.

It is straightforward to show that the projectors B_s and A_p all commute with each other, and that the ground state of Hamiltonian (3) on a planar patch with open boundaries (with suitable boundary conditions) is the unique *equal-weight*

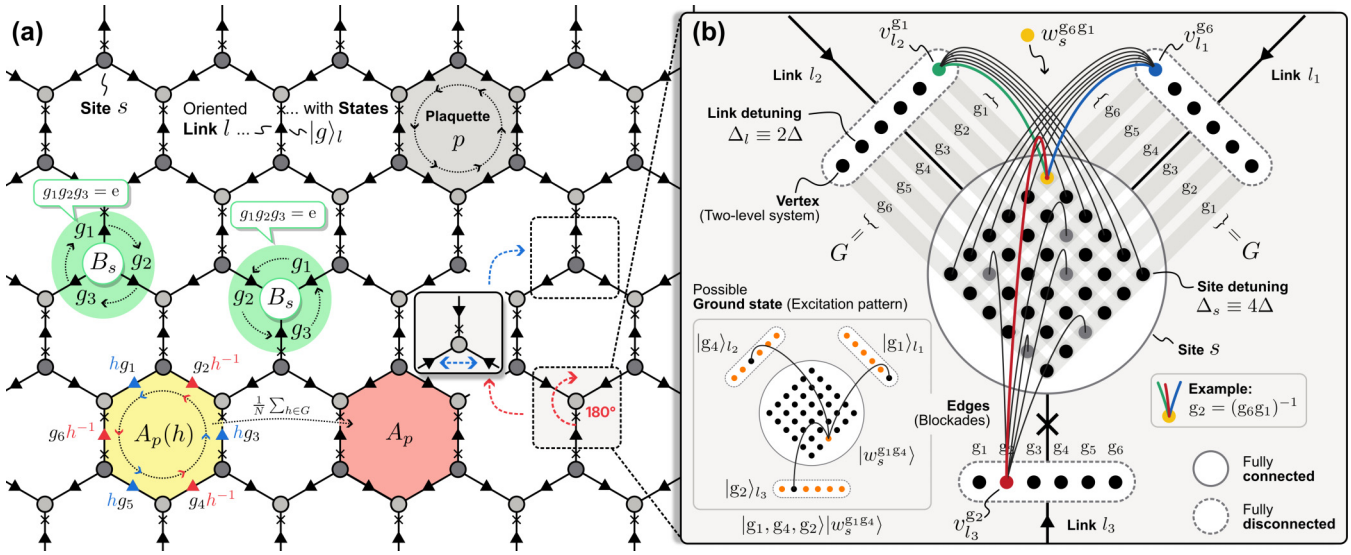

FIG. 1. Conventions and construction. (a) We construct quantum doubles (3) for a finite group G on the trivalent and bipartite honeycomb lattice. By convention, the links of the lattice are assigned an orientation (solid arrows). Every link l is associated with an $N = |G|$-dimensional quantum system with one state $|g\rangle_l$ for each group element $g \in G$. Each plaquette p is assigned a counterclockwise orientation (dotted arrows). With this convention, a plaquette p is on the left (right) of a bounding link l [write $l \in {}_p\!\uparrow$ ($l \in \uparrow_p$)], if the link's orientation is parallel (antiparallel) to the orientation of the plaquette. On each site s, we define a projector B_s that singles out states that satisfy the no-flux condition $g_1g_2g_3 = \mathrm{e}$, where $\mathrm{e} \in G$ denotes the identity and the multiplication sequence depends on the sublattice (two green sites). On each plaquette, there are operators $A_p(h)$ that act by left/right multiplication on the group elements on the bounding links (blue/red). $A_p(h)$ acts by left (right) multiplication if the plaquette orientation aligns (counteraligns) with the link orientation. This construction ensures that $A_p(h)$ commutes with all site constraints $g_1g_2g_3 = \mathrm{e}$ enforced by B_s. Summing over all group elements yields the projector A_p. (b) Microscopically, the quantum double is realized by a blockade Hamiltonian (2) encoded by a blockade graph $\mathcal{G} = (V, E, W)$. Depicted is an example for $N = 6$ with group elements g_i for $i = 1, \ldots, 6$ and an exemplary group product $\mathrm{g}_2 = (\mathrm{g}_6\mathrm{g}_1)^{-1}$. Note that roman symbols like g_2 label *specific group elements*, whereas italic symbols like g_3 are used as *variables*. For the construction, it is convenient to mark one of the three edges at each site (crosses); this choice has no physical meaning. Then one places N two-level systems (vertices) on each link l, which are not in blockade with each other; each is assigned a group element and labeled by v_l^g. Additionally, there are N^2 two-level systems on the site labeled by pairs of group elements and denoted by $w_s^{g_1g_2}$; these site systems are all in blockade with each other (blockades not shown). The crucial part is how the link vertices are connected by edges (blockades) to the site vertices (solid arcs, only a few are shown). This construction is explained in the text and depends on the orientation of the site (= the sublattice) and the marked edge (crosses). The inset shows an exemplary classical ground state $|\mathrm{g}_1, \mathrm{g}_4, \mathrm{g}_2\rangle\, |w_s^{\mathrm{g}_1\mathrm{g}_4}\rangle$ that satisfies all blockades and realizes the state with the constraint $\mathrm{g}_1\mathrm{g}_4\mathrm{g}_2 = \mathrm{e}$. Note that there is only one two-level system excited on the site and all but one on each link. Although the construction seems to break the threefold rotation symmetry of a site (via the edge marked with a cross), the cyclic symmetry of the constraint $g_1g_2g_3 = \mathrm{e}$ ensures that the constructed blockade graph is completely symmetric under rotations by 120°. To obtain the blockade graph on the other sublattice, one can rotate the shown site by 180° and swap two of the three edges, thereby inverting the orientation of the multiplication around the vertex.

superposition of all configurations that satisfy the local constraints imposed by the site terms B_s. For the abelian group $G = \mathbb{Z}_2$, this model yields the toric code on a honeycomb lattice, whereas for a general group G, the ground state is the fixed-point wave function of a topological phase characterized by the quantum double $\mathcal{D}(G)$ of the group G [5,72,73]. Notably, for non-Abelian groups G, these topological phases feature non-Abelian anyonic excitations and can be used for universal topological quantum computation [69]. For more details and a pedagogical introduction to quantum double models we refer the reader to Ref. [67].

C. Quantum doubles with blockade structures

We now describe a construction $G \mapsto \mathcal{G}$ of a blockade graph $\mathcal{G}$ for an arbitrary finite group G, such that the ground state of the associated blockade Hamiltonian (2) for weak $\Omega \ll \Delta_i, U_0$ is in the topological phase of the quantum double Hamiltonian (3). We first explain the rationale of our approach and then describe the detailed construction below.

1. Rationale

We start with $\Omega = 0$ and construct a blockade graph $\mathcal{G} = (V, E, W)$ such that there is a one-to-one correspondence between the degenerate ground states of H_G and H_G for $J_p = 0$ (this ground-state manifold is extensively degenerate). Crucially, the construction of $\mathcal{G}$ ensures the existence of a group of local graph automorphisms that translate to local symmetries of the Hamiltonian H_G. The generators of this local symmetry act on the ground-state space of H_G exactly like the operators $A_p(h)$ act on the ground-state space of H_G (for $J_p = 0$). Then, we turn on a weak field Ω and show that the (now unique) ground state of H_G exhibits topological order and is in the same phase as the ground state of the quantum double H_G for finite $J_p > 0$. Thus, the core idea for this realization of Kitaev's quantum double models is to implement the site

terms B_s via diagonal two-body interactions, while the terms $A_p(h)$ appear as a local symmetry of the microscopic Hamiltonian. Together with a uniform transverse field Ω, the latter implies the perturbative generation of $A_p(h)$-terms in the low-energy effective Hamiltonian of the system. Note that for $G = \mathbb{Z}_2$ this approach leads to the model introduced in Ref. [61], and large parts of the proof of topological order presented there can be straightforwardly generalized to the construction for arbitrary groups G discussed here.

2. A single site

We now describe the construction of the graph $\mathcal{G}$ for the Hamiltonian $H_\mathcal{G}$ in detail. To this end, we consider a finite group G with $N = |G|$ elements. As shown in Fig. 1(b), we distinguish between two-level systems placed on the *links* to implement the logical states $|g\rangle_l$, and two-level systems on the *sites* to realize the site constraints. For simplicity, we start with the construction of a blockade graph $\mathcal{G}_s$ for a single site s of the honeycomb lattice and its three adjacent links, see Fig. 1(b). On the links we place N two-level systems (N *vertices* in graph language). To each vertex on link l we associate a unique group element $g \in G$ and denote this vertex by v_l^g. This yields a Hilbert space of dimension 2^N on each link and we identify the states $|g\rangle_l$ of the quantum double as a basis of an N-dimensional subspace spanned by

$$|g\rangle_l \equiv |\,1\,1\ldots\underset{\substack{\uparrow\\ \text{Vertex } v_l^g}}{0}\ldots 1\,1\,\rangle_l, \tag{4}$$

i.e., all two-level systems on the link are excited to state $|1\rangle$ except for vertex v_l^g, which is in the deexcited state $|0\rangle$. There are no edges (= blockades) connecting the vertices on the links among themselves, and we choose the detunings uniformly, $\Delta_l \equiv \Delta_i = \Delta$ on all vertices of the link. Next, we place N^2 two-level systems with detuning $\Delta_s \equiv \Delta_i = 4\Delta$ on the *site*, such that every pair has a distance smaller than the blockade radius r_B. Hence, the blockade graph on a site with N^2 vertices is *fully connected* and has uniform weight.

The last and most important step is to define the edges of the blockade graph that connect the $3 \times N$ vertices on the three links with the N^2 vertices on their common site. To this end, we label the three links adjacent to site s by l_1, l_2, l_3 with order as indicated in Fig. 1(a), i.e., clockwise for outgoing arrows and counterclockwise for incoming arrows. Furthermore, we assign to each (ordered!) pair of group elements $g_1, g_2 \in G$ a unique vertex on the site s and denote it by $w_s^{g_1 g_2}$. Then the vertex $v_{l_1}^{g_1}$ on the first link connects to the N vertices $w_s^{g_1 h}$ for all $h \in G$, while the vertex $v_{l_2}^{g_2}$ on the second link connects to all vertices $w_s^{h g_2}$ for $h \in G$. Finally, the vertex $v_{l_3}^{g_3}$ on the third link connects to all vertices $w_s^{g_1 g_2}$ that satisfy the condition $g_3 = (g_1 g_2)^{-1}$. Note that for every $g_3 \in G$, there are exactly N vertices on the site that satisfy this condition. In summary, each vertex $w_s^{g_1 g_2}$ on a site has an edge with one vertex on each adjacent link: $v_{l_1}^{g_1}$, $v_{l_2}^{g_2}$, and $v_{l_3}^{g_3}$, with the three group elements satisfying $g_1 g_2 g_3 = \mathrm{e}$. It is important to point out that this construction is invariant under cyclic permutations of the links, since $g_1 g_2 g_3 = g_2 g_3 g_1 = g_3 g_1 g_2$, i.e., the construction is invariant under the choice of labeling. In particular, the (apparent) distinction of one of the three links [Fig. 1(b)] is an artifact of the construction and not reflected in the graph. Furthermore, a mapping between sites with incoming arrows and sites with outgoing arrows is possible by exchanging the labeling between two links.

For such a single site with three adjacent links, the ground states of the Hamiltonian $H_{\mathcal{G}_s}^0$ (with $U_0 > \Delta_s$) are characterized by a single vertex $w_s^{g_1 g_2}$ in state $|1\rangle$ and all other vertices on the site in state $|0\rangle$ due to the on-site blockade interactions; we denote this state by $|w_s^{g_1 g_2}\rangle$. Meanwhile, on each adjacent link, the (unique) vertex connected to the excited vertex $w_s^{g_1 g_2}$ is in state $|0\rangle$ because of the blockade, while all other vertices on the link are in state $|1\rangle$. Therefore, each link is in state $|g_l\rangle_l$ with the constraint $g_1 g_2 g_3 = \mathrm{e}$. Hence, all states in the degenerate ground-state manifold of a single site can be written as $|g_1, g_2, g_3\rangle\,|w_s^{g_1 g_2}\rangle$ with $g_1 g_2 g_3 = \mathrm{e}$, and there is a one-to-one correspondence to the eigenstates of the projection operator B_s with eigenvalue $+1$ of the quantum double (3). The ground-state energy of $H_{\mathcal{G}_s}^0$ for a single site with three links is $E = -(3N+1)\Delta$. It is important to stress that here the full Hilbert space of a site with three links is 2^{3N+N^2}-dimensional and therefore much larger than the Hilbert space of a quantum double model with dimension N^3. In particular, the one-to-one mapping is only valid for *ground states*, while our blockade model has a much richer excitation structure.

3. Graph automorphisms of a single site

Before we extend this analysis to the full honeycomb lattice, we discuss the *graph automorphisms* of such a single site (and its three adjacent links). Automorphisms of vertex-weighted graphs are permutations of vertices that map adjacent vertices to adjacent vertices with the same weights. The set of all automorphisms of a graph forms its *automorphism group* (with concatenation of automorphisms as the multiplication). Because of the high symmetry of the construction, the automorphism group of the graph $\mathcal{G}_s$ turns out to be $(G \times G) \rtimes \mathrm{Aut}(G)$ with $\mathrm{Aut}(G)$ the group of group automorphisms of G. In the following, we focus on an important subgroup of these graph automorphisms; a discussion of the full automorphism group can be found in Sec. S1 of the Supplemental Material (SM) [74].

Since each vertex on a link is associated with a unique group element $g \in G$, the group G induces a permutation $\varphi_l(h,k)$ of vertices on link l via

$$\varphi_l(h,k) : v_l^g \mapsto v_l^{hgk^{-1}} \quad \text{for every } h,k \in G. \tag{5}$$

Note that these permutations map the states $|g\rangle_l$ on link l to the states $|hgk^{-1}\rangle_l$ on the same link. Correspondingly, there is a permutation $\phi_s(h_1,h_2,h_3)$ of the vertices on site s defined via

$$\phi_s(h_1,h_2,h_3) : w_s^{g_1 g_2} \mapsto w_s^{h_1 g_1 h_2^{-1}\, h_2 g_2 h_3^{-1}} \tag{6}$$

for every triple $h_1, h_2, h_3 \in G$. The permutations (5) and (6) allow us to define a permutation Φ_s, which acts on the vertices of site s and all three adjacent links, and turns out to be a graph automorphism of $\mathcal{G}_s$ parametrized by three group elements,

$$\begin{aligned}\Phi_s(h_1,h_2,h_3) := {} & \varphi_{l_1}(h_1,h_2)\cdot\varphi_{l_2}(h_2,h_3)\cdot\varphi_{l_3}(h_3,h_1) \\ & \times \phi_s(h_1,h_2,h_3).\end{aligned} \tag{7}$$

Crucially, the automorphism Φ_s leaves the constraint $g_1g_2g_3 = \mathrm{e}$ invariant. Note that every permutation of vertices (two-level systems) induces a unitary operator on the Hilbert space; by abuse of notation, we denote permutations and induced unitaries with the same symbol. Then the (unitary action of) Φ_s maps ground states of $H^0_{\mathcal{G}_s}$ onto each other. In addition, these operations generate a single *orbit*, i.e., starting from an arbitrary ground state $|g_1, g_2, g_3\rangle\,|w_s^{g_1g_2}\rangle$ one can reach any other ground state by applying these graph automorphisms. According to the definition put forward in Ref. [61], this makes the blockade structure $\mathcal{G}_s$ *fully symmetric*, a special feature that ensures that the ground states of $H_{\mathcal{G}_s}$ for $\Omega \neq 0$ contain *equal-weight superpositions* of the degenerate ground states of $H^0_{\mathcal{G}_s}$. Of special interest in the following are graph automorphisms $\Phi_s(h) \equiv \Phi_s(\mathrm{e}, h, \mathrm{e})$ with two elements h_i equal to the identity e. Under these permutations, the state $|g\rangle_{l_3}$ on one link (here l_3) remains invariant, whereas the other two links (here l_1 and l_2) transform as $\Phi_s(h)\,|g\rangle_{l_1} = |gh^{-1}\rangle_{l_1}$ and $\Phi_s(h)\,|g\rangle_{l_2} = |hg\rangle_{l_2}$, respectively. These automorphisms allow us to construct local *plaquette automorphisms* below.

4. Tessellation on the honeycomb lattice

We close this section by constructing the blockade graph $\mathcal{G}$ on the full honeycomb lattice. The most important aspect is that the orientation of the sites of the honeycomb lattice alternates between *clockwise* (outgoing arrows) and *counterclockwise* (incoming arrows), Fig. 1(a). The construction of both types of sites follows the recipe detailed above: For each site, we label the adjacent links according to its orientation, and connect the vertices on the links to the vertices on the site as explained above. The site graphs are then joined by identifying the vertices on common links. To ensure that this construction leads to a gapped ground-state manifold that realizes the intended constraints on every site, one adds up the detunings of vertices that are shared between sites. This leads to the link detunings $\Delta_l = 2\Delta$ in the bulk of the honeycomb lattice. A mathematically rigorous discussion of this construction (*amalgamation*) can be found in Ref. [60]. Note that for *open* boundaries, the above procedure leads to link detunings $\Delta_l = 2\Delta$ in the bulk, but only $\Delta_l = 1\Delta$ for dangling links on the boundary.

In summary, this construction provides the required graph $\mathcal{G}$ describing the Hamiltonian $H_{\mathcal{G}}$ in Eq. (2). The remainder of this paper is dedicated to studying the ground-state properties of $H_{\mathcal{G}}$ and discussing local modifications needed for braiding anyons. As a final remark, we point out that a similar construction—which gives rise to the same local permutation symmetry—was recently proposed by Yu *et al.* [41]. However, their Hamiltonian is not a natural fit for the Rydberg platform, as it relies on an intricate pattern of ferromagnetic and antiferromagnetic spin couplings; the Hamiltonians studied in Ref. [41] and the blockade Hamiltonians $H_{\mathcal{G}}$ are therefore different, though closely related.

III. GROUND-STATE PROPERTIES

A. Ground-state manifold for $\Omega = 0$

The graph $\mathcal{G}$ on a honeycomb lattice with periodic boundary conditions and A unit cells contains $|V| = (3N + 2N^2)A$ vertices, so that the Hilbert space $\mathcal{H}_{\mathcal{G}}$ of our model is $2^{|V|}$-dimensional. The ground-state manifold $\mathcal{H}^0_{\mathcal{G}}$ of $H^0_{\mathcal{G}}$ for $U_0 > 4\Delta$ is characterized by a state $|g_l\rangle_l$ on each link, and a state $|w_s^{g_ig_j}\rangle$ on each site, such that the group elements on the links $\boldsymbol{g} \equiv \{g_l\}$ satisfy the constraints of the projectors B_s for all sites (namely $g_1g_2g_3 = \mathrm{e}$ for the three links connected to a site). We denote states that satisfy this constraint on all sites as $|\boldsymbol{g}\rangle$; they span the ground-state manifold $\mathcal{H}^0_{\mathcal{G}}$. States in the orthogonal complement $\mathcal{H}^\perp_{\mathcal{G}} \equiv (\mathcal{H}^0_{\mathcal{G}})^\perp$ are denoted by $|\boldsymbol{n}\rangle$. This demonstrates the one-to-one mapping between $\mathcal{H}^0_{\mathcal{G}}$ and the degenerate ground states of the quantum double Hamiltonian H_G for $J_p = 0$. Note that all states $|\boldsymbol{n}\rangle \in \mathcal{H}^\perp_{\mathcal{G}}$ exhibit an excitation gap of at least 2Δ.

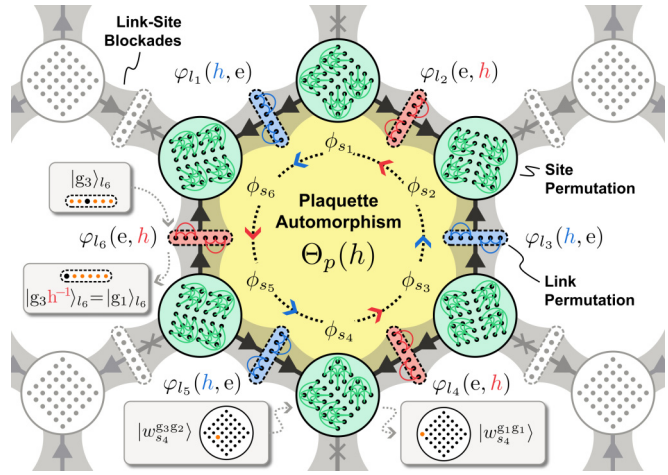

FIG. 2. Plaquette automorphisms. The blockade graph $\mathcal{G}$ (shaded gray) constructed in Fig. 1 allows for local automorphisms $\Theta_p(h)$ for each $h \in G$ that affect only the vertices on links and sites bounding a single plaquette p. The automorphism decomposes into a product of permutations of vertices φ_l and ϕ_s on links $l \in p$ and sites $s \in p$, respectively. The link permutations depend on whether the link orientation is parallel (antiparallel) to the orientation of the plaquette (blue and red arrows). The definition of these permutations is given in the text. Describing the site permutations ϕ_s is most convenient if the site vertices are labeled by the pairs of group elements of the two adjacent edges that bound the plaquette. (To apply the construction detailed in Sec. II, the radial edge on every site of the plaquette is identified with l_3 [marked by a cross]; this is indicated by rotated and mirrored arrays of site vertices.) As a blockade graph automorphism, $\Theta_p(h)$ induces a symmetry of the blockade Hamiltonian $H_{\mathcal{G}}$ on the full Hilbert space. As such, the ground-state manifold remains invariant, and the representation induced by the link permutations acts by left and right group multiplications on the ground states $|\boldsymbol{g}\rangle$ in $\mathcal{H}^0_{\mathcal{G}}$. The insets show exemplary actions of the permutations on states (black vertices: $|0\rangle$, orange vertices: $|1\rangle$). Note that links (and sites) that are not adjacent to p are unaffected by the automorphism (gray).

B. Plaquette automorphisms

Next, we show the existence of local graph automorphisms on each plaquette (Fig. 2); the complete automorphism group for periodic boundaries is discussed in Sec. S2 of the SM [74]. For each group element $h \in G$, we can define a permutation $\Theta_p(h)$ of vertices that belong to the links and sites surrounding a single plaquette p. To define $\Theta_p(h)$, we choose a labeling for

each affected site s such that l_3 is the link that points outwards (is not part of the plaquette). Then the permutation is defined via the permutations (5) and (6) as

$$\Theta_p(h) := \prod_{l\in\uparrow_p} \varphi_l(\mathrm{e}, h) \prod_{l'\in_p\uparrow} \varphi_{l'}(h, \mathrm{e}) \prod_{s\in p} \phi_s(\mathrm{e}, h, \mathrm{e}), \tag{8}$$

where $\uparrow_p$ ($_p\uparrow$) labels the links with the plaquette to the right (left) of the arrow, and $s \in p$ denotes sites on the boundary of plaquette p. It is easy to convince oneself that this permutation is a local graph automorphism of $\mathcal{G}$ for every $h \in G$. To see this, recall that every *single* site graph $\mathcal{G}_s$ has automorphisms $\Phi_s(\mathrm{e}, h, \mathrm{e})$, which leave one link ($l_3$) invariant. $\Theta_p(h)$ is the result of chaining six of these permutations along common links bounding a plaquette. Hence, we refer to $\Theta_p(h)$ as *plaquette automorphisms*. Remarkably, plaquette automorphisms on different plaquettes commute with each other—in analogy with the operators $A_p(h)$ of the quantum double model (3). Since $\Theta_p(h)$ is an automorphism of $\mathcal{G}$, the induced unitary representation [which we also denote by $\Theta_p(h)$] gives rise to a local symmetry of the blockade Hamiltonian $H^0_{\mathcal{G}}$, i.e.,

$$\Theta_p(h) H^0_{\mathcal{G}} = H^0_{\mathcal{G}} \Theta_p(h) \quad \text{for all plaquettes } p \text{ and } h \in G.$$

As a consequence, all $\Theta_p(h)$ leave the ground-state manifold $\mathcal{H}^0_{\mathcal{G}}$ invariant and act on ground states $|\boldsymbol{g}\rangle$ exactly like the operators $A_p(h)$ act on the corresponding ground states of the quantum double model (3) for $J_p = 0$. However, in contrast to the operators $A_p(h)$, the operators $\Theta_p(h)$ affect not only states on links but also states on sites, and furthermore act nontrivially on excited states $|\boldsymbol{n}\rangle \in \mathcal{H}^{\perp}_{\mathcal{G}}$.

C. Ground-state manifold for $\Omega \neq 0$

We can now discuss the ground state of the full Hamiltonian $H_{\mathcal{G}}$ with finite transverse field $\Omega \neq 0$. Note that for uniform Ω [recall Eq. (2)] the operators $\Theta_p(h)$ remain symmetries of the full Hamiltonian $H_{\mathcal{G}}$. When a finite patch of the honeycomb lattice is embedded on a topologically trivial surface with open boundaries (and "dangling" edges), the plaquette automorphisms $\Theta_p(h)$ map all states $|\boldsymbol{g}\rangle$ in the ground-state manifold $\mathcal{H}^0_{\mathcal{G}}$ onto each other. This follows from the analogous property of Kitaev's quantum double models [5,71]. Thus, the graph automorphisms $\Theta_p(h)$ generate a single orbit, and the complete blockade structure described by $\mathcal{G}$ is fully symmetric (for details see Sec. S3 of the SM [74]). This allows us to apply Theorem 1 from Ref. [61], which states that in this case the ground state $|\Omega\rangle$ of $H_{\mathcal{G}}$ is unique and has the form

$$|\Omega\rangle = \lambda(\Omega) \sum_{|\boldsymbol{g}\rangle\in\mathcal{H}^0_{\mathcal{G}}} |\boldsymbol{g}\rangle + \sum_{|\boldsymbol{n}\rangle\in\mathcal{H}^{\perp}_{\mathcal{G}}} \eta_{\boldsymbol{n}}(\Omega)\,|\boldsymbol{n}\rangle\,. \tag{9}$$

The first term describes an equal-weight superposition of all product-basis states $|\boldsymbol{g}\rangle$ in $\mathcal{H}^0_{\mathcal{G}}$, while the second term describes admixtures of additional states because of the transverse field. Note that the ground state (9) is in the subspace $\mathcal{H}^S_{\mathcal{G}}$ (*symmetric sector*) of all states with eigenvalue $+1$ for all symmetries $\Theta_p(h)$, i.e.,

$$|\Omega\rangle \in \mathcal{H}^S_{\mathcal{G}} = \{\,|\psi\rangle \,|\, \forall p, h : \Theta_p(h)|\psi\rangle = |\psi\rangle\,\} < \mathcal{H}_{\mathcal{G}}. \tag{10}$$

For *periodic* boundary conditions, there is also a unique ground state in the symmetric sector. However, equal-weight superpositions of states in $\mathcal{H}^0_{\mathcal{G}}$ are only guaranteed within the orbits generated by blockade-graph automorphisms {which are generated by plaquette automorphisms (8) and additional nonlocal automorphisms, see [75] and Sec. S2 of the SM [74]}.

We stress that, because of the admixtures in Eq. (9), one cannot immediately conclude that $|\Omega\rangle$ is topologically ordered. However, for weak $\Omega \ll \Delta$, we can follow the arguments from Ref. [61] to show that the state (9) is topologically ordered and characterized by the quantum double model $\mathcal{D}(G)$. The rigorous proof for $G = \mathbb{Z}_2$ is given in Ref. [61] and its extension to arbitrary groups G is detailed in Appendix A. Here, we only sketch the gist of the proof. It requires periodic boundary conditions and makes use of the extended auxiliary Hamiltonian

$$\tilde{H}_{\mathcal{G}}(\Omega, \omega) := H^0_{\mathcal{G}} + \Omega \sum_{i\in V} \sigma^x_i + \omega \sum_{\text{Faces } p} \left[\mathbb{1} - \overbrace{\frac{1}{|G|} \sum_{h\in G} \Theta_p(h)}^{\text{Projector } \Theta_p} \right]. \tag{11}$$

For $\omega = 0$ and $\Omega = 0$, we recover the extensive ground-state degeneracy of $\mathcal{H}^0_{\mathcal{G}}$ (now with topological degeneracies). In a first step, we turn on ω with $0 < \omega < \Delta$. This lifts the extensive degeneracy and the ground states become equal-weight superpositions of states $|\boldsymbol{g}\rangle$ in the orbits generated by plaquette symmetries $\Theta_p(h)$. The new ground-state manifold $\mathcal{H}^{\omega}_{\mathcal{G}} = \mathcal{H}^0_{\mathcal{G}} \cap \mathcal{H}^S_{\mathcal{G}}$ has only topological degeneracies and is separated by a finite excitation gap of order ω from excited states. The ground states in $\mathcal{H}^{\omega}_{\mathcal{G}}$ can be mapped by local unitaries to the ground states of Kitaev's quantum double model (3) and are therefore topologically ordered; note that they are also in the symmetric sector $\mathcal{H}^S_{\mathcal{G}}$ since $\Theta_p(h)\Theta_p = \Theta_p$ for all $h \in G$. The ground-state manifold $\mathcal{H}^{\omega}_{\mathcal{G}}$, together with the Hamiltonian $\tilde{H}_{\mathcal{G}}(0, \omega)$, shows that the latter is *frustration free* and satisfies a condition called *local topological quantum order* [76–78]. Given these features, it can be shown that its gap is stable in the thermodynamic limit against arbitrary, small, local perturbations [77], which implies that the ground-state manifold remains in the same gapped topological phase [79]. In particular, we can turn on a small transverse field $\Omega \ll \omega, \Delta$ and the new ground-state manifold $\mathcal{H}^{\Omega,\omega}_{\mathcal{G}}$ of the Hamiltonian $\tilde{H}_{\mathcal{G}}(\Omega, \omega)$ remains topologically ordered. (Note that the topological ground-state degeneracy can be lifted by finite size effects.) Using the arguments from above, we know that $H_{\mathcal{G}}$ has a unique ground state $|\Omega\rangle$ in the symmetric sector $\mathcal{H}^S_{\mathcal{G}}$. Since $H_{\mathcal{G}}$ commutes with $\tilde{H}_{\mathcal{G}}(\Omega, \omega)$ and $|\Omega\rangle$ is annihilated by the positive-semidefinite auxiliary term in Eq. (11), $|\Omega\rangle$ must also be the (unique) ground state of $\tilde{H}_{\mathcal{G}}(\Omega, \omega)$, i.e., $|\Omega\rangle \in \mathcal{H}^{\Omega,\omega}_{\mathcal{G}}$. This demonstrates that the ground state $|\Omega\rangle$ of $H_{\mathcal{G}}$ for small enough $\Omega \ll \Delta$ is in the same topological phase as Kitaev's quantum double model (3).

The gap stability argument above also implies an excitation gap of order Δ to all states in the symmetric sector $\mathcal{H}^S_{\mathcal{G}}$ (this includes "flux excitations" of the quantum double, see Sec. IV below). Consequently, the ground states are protected by a gap against any perturbation that respects the plaquette symmetries $\Theta_p(h)$. An important question is whether the Hamiltonian

$H_\mathcal{G}$ also exhibits a gap between states in the symmetric sector $\mathcal{H}^S_\mathcal{G}$ and its complement $(\mathcal{H}^S_\mathcal{G})^\perp$ (this includes "charge excitations"). Such a gap is at least suggested by a (heuristic) Schrieffer–Wolff transformation [80] that predicts an effective Hamiltonian within the manifold $\mathcal{H}^0_\mathcal{G}$ of the form

$$H_{\text{eff}} \sim -\Delta_c \sum_p \sum_{h\in G\setminus\{\text{e}\}} \Theta_p(h) \tag{12}$$

with coupling $\Delta_c \sim \Delta(\frac{\Omega}{\Delta})^K$ and K the number of two-level systems that flip their state under the action of $\Theta_p(h)$ (i.e., $K = 24$ for the honeycomb lattice). However, a rigorous proof of the existence of a finite charge gap is technically challenging and is deferred to an upcoming paper [62].

In the following (second) part of this paper, we modify the blockade Hamiltonian to prepare localized fluxes and explore adiabatic preparation and braiding schemes. Because of these modifications, the rigorous arguments discussed up to this point (underlying topological order and gap stability) do *not* carry over. The following results and claims *are* rigorous if one prepares the system in the symmetric sector and switches off quantum fluctuations (since then the system is described by quantum double fixed point wave functions). We expect, of course, that these fixed point properties remain robust in the presence of finite quantum fluctuations—but this remains mathematically unproven.

IV. FLUX ANYONS AND WILSON LOOPS

A. Review: Anyons of $\mathcal{D}(G)$

The types of anyonic excitations of the quantum double $\mathcal{D}(G)$ are classified by the irreducible representations of the Drinfeld double [5,81]. A systematic characterization of the anyons is given by the following construction [67,72]. First, one picks a conjugacy class C of the group G with an arbitrary representative $r_C \in C$, i.e., $C = \{gr_Cg^{-1} \,|\, g \in G\}$. Next, one considers the centralizer $Z_G(r_C) = \{g \in G \,|\, gr_C = r_Cg\}$ of this representative, i.e., the subgroup of G of all elements that commute with r_C. The different anyon types of the quantum double $\mathcal{D}(G)$ can then be labeled by pairs $[C, R]$ of a conjugacy class C and an irreducible representation R of its centralizer $Z_G(r_C)$. (Note that the irreducible representations are independent of the representative r_C since centralizers of different representatives are isomorphic via conjugation.) The quantum dimension $d_{[C,R]}$ of an anyon turns out to be the product of the number of elements in the conjugacy class C and the dimension d_R of the irreducible representation R: $d_{[C,R]} = |C|d_R$. Following the nomenclature of a lattice gauge theory, one distinguishes *flux anyons* $[C, E]$ given by a conjugacy class C and the trivial representation E, and *charge anyons* $[C_\text{e}, R]$ given by an irreducible representation R of the group $G = Z_G(\text{e})$ and the conjugacy class $C_\text{e} \equiv \{\text{e}\}$ of the identity; anyons $[C, R]$ with $C \neq C_\text{e}$ and $R \neq E$ carry flux and charge and are referred to as *dyons*.

B. Preparing flux anyons with blockade structures

The Hamiltonian $H_\mathcal{G}$ with its blockade graph $\mathcal{G}$ [defined via the site graphs $\mathcal{G}_s$, recall Fig. 1(b)] enforces the zero-flux constraint $g_1g_2g_3 = \text{e}$ on every site by construction. This means that flux excitations (which violate this constraint)

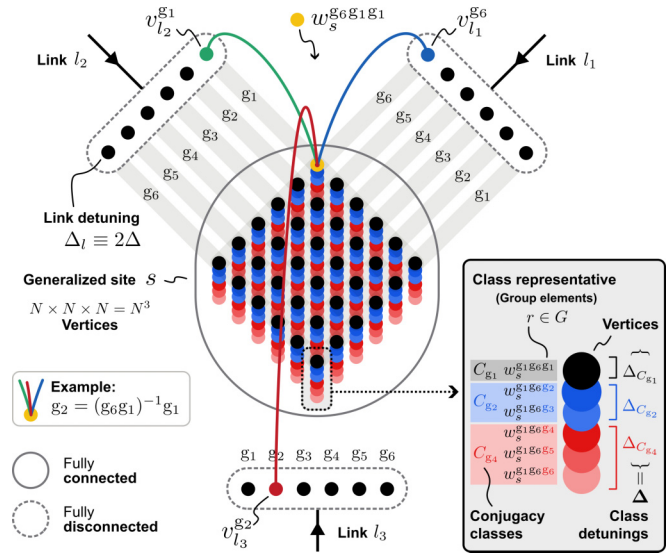

FIG. 3. Generalized site graph. Generalized blockade graph $\mathcal{G}_s[\boldsymbol{\Delta}]$ for a single site s of the honeycomb lattice [cf. Fig. 1(b)]. The site allows for the control of the energy of the configurations on adjacent links $l_{1,2,3}$, which multiply into a prescribed conjugacy class C_r of G: $g_1g_2g_3 = r$ with $r \in C_r$. (This corresponds to a flux anyon $[C_r, E]$ on the vertex.) Here, we assume G has three conjugacy classes: $C_{\text{g}_1} = \{\text{g}_1\}$, $C_{\text{g}_2} = \{\text{g}_2, \text{g}_3\}$, and $C_{\text{g}_4} = \{\text{g}_4, \text{g}_5, \text{g}_6\}$. Note that every vertex on the site is in blockade with all other vertices on the site and with exactly one vertex on each adjacent link (only the blockades of the vertex $w_s^{\text{g}_6\text{g}_1\text{g}_1}$ are shown). That the detunings are uniform for all layers that belong to the same conjugacy class is crucial for full symmetry. This construction can be used as a "flux factory" for adiabatically preparing and pinning arbitrary flux anyons on the site. The detailed construction is explained in the text.

are energetically penalized. In the following, we present a straightforward generalization of the site graph $\mathcal{G}_s$ that allows for the preparation of states with an arbitrary flux anyon trapped on site s, while maintaining a well-defined excitation gap to other flux sectors (and the vacuum). As explained above, flux anyons $[C, E]$ are characterized by a conjugacy class C of the group G. One can create such a localized flux on a given site s by enforcing the modified constraint $g_1g_2g_3 \in C$ on the three links connected to this site. In the following, we describe a generalization $\mathcal{G}_s[\boldsymbol{\Delta}]$ of the site graph $\mathcal{G}_s$, which allows for the preparation of any flux anyon $[C, E]$ on site s in the ground state (Fig. 3). Instead of $N^2 = |G|^2$ two-level systems on the site, we now need N^3 two-level systems, all of which are in blockade, so that the induced graph is fully connected and only one of these two-level systems can be excited at any time; we label these vertices by $w_s^{g_1g_2r}$ with $g_1, g_2, r \in G$. Next, we choose detunings $\boldsymbol{\Delta} \equiv \{\Delta_C\}$ for all conjugacy classes C of G; these determine by how much the energy of a flux anyon $[C, E]$ on this site is lowered, and therefore play the role of site-local chemical potentials for flux anyons. To this end, we set the detuning of vertex $w_s^{g_1g_2r}$ to Δ_C, where C is the conjugacy class of r (i.e., $r \in C$), such that for every conjugacy class C there are $|C|N^2$ vertices with the same detuning Δ_C. We can now define the edges of the graph $\mathcal{G}_s[\boldsymbol{\Delta}]$ that connect the vertices on the adjacent links to the

vertices on the site. Each vertex $v_{l_1}^{g_1}$ on link l_1 is connected to the N^2 vertices $w_s^{g_1 hr}$ on the site, while each vertex $v_{l_2}^{g_2}$ on link l_2 is connected to the N^2 vertices $w_s^{hg_2 r}$. Finally, we connect every vertex $w_s^{g_1 g_2 r}$ on the site to the vertex $v_{l_3}^{g_3}$ on link l_3 with $g_3 = (g_1 g_2)^{-1} r$. As a consequence, each configuration that satisfies the constraint $g_1 g_2 g_3 \in C$, with C a conjugacy class of G, has the same energy contribution $-\Delta_C$. To prepare a specific flux anyon $[C_r, E]$ on such a site, one sets $\Delta_{C_r} = 4\Delta$ and $\Delta_C = -\Delta$ for all $C \neq C_r$. This lowers the energy of the flux anyon $[C_r, E]$ and separates it by a gap from all other flux excitations (and the vacuum). It is crucial that this site graph respects all local graph automorphisms of $\mathcal{G}_s$ discussed in Sec. II, and that a Hamiltonian $H_{\tilde{\mathcal{G}}}$ derived from a graph $\tilde{\mathcal{G}}$ that uses the generalized site graph $\tilde{\mathcal{G}}_s[\mathbf{\Delta}_s]$ on some sites (with potentially different detunings $\mathbf{\Delta}_s$) is still symmetric under the local plaquette automorphisms $\Theta_p(h)$ introduced in Sec. III. Only global symmetries derived from outer automorphisms of G are modified by this construction; for details see Sec. S1 of the SM [74].

By construction, the ground states of the Hamiltonian $H_{\tilde{\mathcal{G}}}^0$ in the symmetric sector $\mathcal{H}_{\tilde{\mathcal{G}}}^S$ are described by flux anyons trapped on the sites with a generalized site graph $\mathcal{G}_s[\mathbf{\Delta}_s]$, and their energy can be tuned by the detunings $\mathbf{\Delta}_s$. It is important to point out that the ground-state manifold of a system with nontrivial flux anyons can have a topological ground-state degeneracy even on topologically trivial surfaces. Furthermore, there is a finite excitation gap to states within the symmetric sector $\mathcal{H}_{\tilde{\mathcal{G}}}^S$. Therefore, this construction can be used to prepare states with a preferred flux pattern on the lattice as *ground states* of the blockade Hamiltonian $H_{\tilde{\mathcal{G}}}^0$. We will use this feature in Sec. V to implement the braiding of flux anyons. Note that the above construction can be significantly simplified if the goal is to trap a *specific* flux anyon $[C_r, E]$. In this case, one can omit all site vertices except the $|C_r|N^2$ vertices that belong to the relevant conjugacy class (and, if required, the N^2 vertices for the vacuum C_e).

Following the discussion in Sec. III on the robustness of topological order for a finite transverse field $\Omega \neq 0$ in a flux-free state on a torus, we expect that the topological properties and ground-state degeneracy of the modified Hamiltonian $H_{\tilde{\mathcal{G}}}$ in the symmetric sector $\mathcal{H}_{\tilde{\mathcal{G}}}^S$ are again robust in the presence of a small but finite transverse field $\Omega \neq 0$, even in the presence of imprinted flux anyons. In this case, the splitting of the ground-state degeneracy is exponentially suppressed in the distance between the flux anyons (instead of the system size) and therefore requires that flux anyons are far apart.

C. Probing flux anyons with Wilson loops

In analogy to lattice gauge theories, the flux anyons are conveniently probed and characterized by *Wilson loops*. In the case of quantum doubles, Wilson loops are closely related to closed charge-like *Ribbon operators,* which probe the enclosed flux [5,67]. Wilson loop operators are associated to a closed, oriented loop γ on the *dual* lattice, see Fig. 4. In the product basis $|\boldsymbol{g}\rangle \in \mathcal{H}_G$ of the quantum double model (3), they

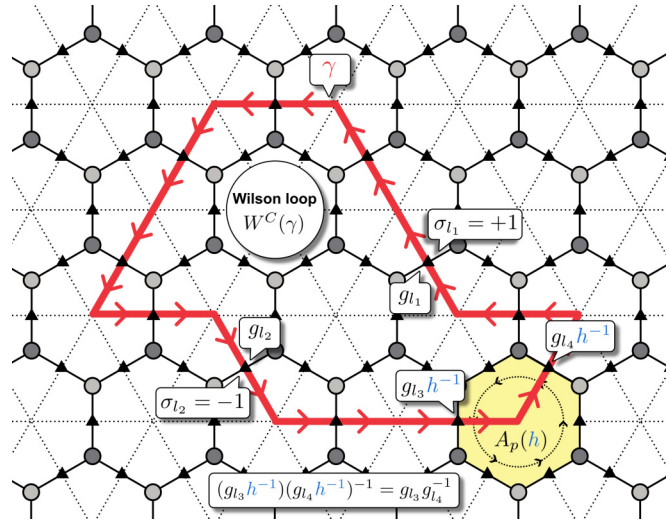

FIG. 4. Wilson loops. Wilson loop operators $W^C(\gamma)$ are defined on closed, oriented loops γ (red) on the dual lattice (dotted). For the evaluation of $W^C(\gamma)$ in the product basis $|\boldsymbol{g}\rangle \in \mathcal{H}_G$, the product of all group elements $g_l^{\sigma_l}$ on links l crossed by γ is needed (with multiplication order from left to right along the loop's orientation); here $\sigma_l = +1$ ($\sigma_l = -1$) if the crossed edge l points to the left (right) of γ when following its orientation. This construction ensures that $W^C(\gamma)$ commutes with the plaquette operators $A_p(h)$ (plaquette in the bottom right corner).

are defined by

$$W^R(\gamma) := \chi_R\Big(\prod_{l\in\gamma} g_l^{\sigma_l}\Big) \tag{13}$$

with R an irreducible representation of the group G and χ_R its character. The product runs over all links crossed by the closed loop γ (with multiplication order from left to right along the loop's orientation). The exponents $\sigma_l \in \{-1, 1\}$ are defined such that $\sigma_l = +1$ ($\sigma_l = -1$) if the arrow of the crossed link points left (right) when following the loop along its orientation. This convention ensures that $W^R(\gamma)$ commutes with all plaquette operators $A_p(h)$ (Fig. 4).

For fixed point ground states of a quantum double model—which in our case correspond to the ground states of $\tilde{H}_{\tilde{\mathcal{G}}}(0, \omega)$ or, equivalently, the ground states of $H_{\tilde{\mathcal{G}}}^0$ in the symmetric sector—the Wilson loops (13) are independent of the shape of the loop, and only depend on the enclosed flux. For example, a loop γ that encloses a flux $[C, E]$ yields $\langle W^R(\gamma)\rangle = \chi_R(r_C)$ with $r_C \in C$, i.e., the measurement over all irreducible representations R uniquely determines the enclosed flux. This property can be made explicit by taking the discrete Fourier transform of the Wilson loop $W^R(\gamma)$ over the group G,

$$W^C(\gamma) := \frac{1}{|G|}\sum_R \sum_{r\in C} \chi_R^*(r) W^R(\gamma) \tag{14a}$$

$$= \begin{cases} 1 & \text{if } \prod_{l\in\gamma} g_l^{\sigma_l} \in C, \\ 0 & \text{otherwise,} \end{cases} \tag{14b}$$

and therefore $\langle W^{C'}(\gamma)\rangle_C = \delta_{C,C'}$, where $\langle\bullet\rangle_C$ denotes a state with flux C enclosed by γ; see Appendix B for details.

However, in general there are fluctuations of flux excitations. In this case it is known from pure gauge theories in $2+1$ dimensions [82] that the Wilson loop in the trivial phase decays with an area law, whereas in the topological phase it decays with a perimeter law

$$\langle W^R(\gamma)\rangle \sim e^{-|\gamma|/\xi_R}, \tag{15}$$

where $|\gamma|$ denotes the length of γ. Hence the expectation values of Wilson loops can be used to probe two properties: Varying the loop γ and verifying the perimeter law demonstrates the topological character of the phase, and the expectation value for a fixed loop yields information about the enclosed flux.

However, for our implementation of quantum doubles via a Hamiltonian $H_{\tilde{\mathcal{G}}}$ with finite transverse field $\Omega \neq 0$, we cannot necessarily associate a group element g_l with each link, since the full Hilbert space of a link is much larger than $\mathcal{H}_l^G \equiv \mathrm{span}\{\,|g\rangle_l \,|\, g \in G\,\}$. To solve this problem, we modify the Wilson loop operator,

$$\mathbb{W}^R(\gamma) := W^R(\gamma)\prod_{l\in\gamma}\mathbb{P}_l^G, \tag{16}$$

where $\mathbb{P}_l^G$ is the projector on link l onto the subspace $\mathcal{H}_l^G$. This modification guarantees that the Wilson loop operator $\mathbb{W}^R(\gamma)$ is well defined on the full Hilbert space $\mathcal{H}_{\tilde{\mathcal{G}}}$ of the blockade structure $H_{\tilde{\mathcal{G}}}$. To understand the effect of this projector, we consider a simplified model where each link is with probability $p<1$ in a state in $\mathcal{H}_l^G$. Then, the projector $\prod_{l\in\gamma}\mathbb{P}_l^G$ leads to an additional contribution of $p^{|\gamma|}$ to the perimeter law. This suggests that the modified Wilson loop (16) can still distinguish between the trivial and the topological phase, as this additional factor is consistent with a perimeter law. Furthermore, we expect that one can factor out this additional contribution by evaluating the ratio between two Wilson loops with irreducible representation R and trivial representation E, respectively,

$$\overline{\mathbb{W}}^R(\gamma) := \frac{\langle \mathbb{W}^R(\gamma)\rangle}{\langle \mathbb{W}^E(\gamma)\rangle} \approx \frac{1}{|\mathcal{I}_G|}\sum_{\boldsymbol{g}_\gamma\in\mathcal{I}_G}\chi_R\Big(\prod_{l\in\gamma} g_l^{\sigma_l}\Big). \tag{17}$$

Here, $\boldsymbol{g}_\gamma \equiv (g_l)_{l\in\gamma}$ denotes measurement outcomes of one experimental sample for links along the loop γ. The last equality shows that it is convenient for an experiment to evaluate the expectation value by only taking into account the postselected measurements $\mathcal{I}_G$, where all links along the loop γ are in a state in $\mathcal{H}_l^G$.

Finally, we point out that if perturbations of the Hamiltonian $H_{\tilde{\mathcal{G}}}$ slightly break the local symmetries $\Theta_p(h)$, charges are also allowed to fluctuate. To identify the topological phase in this case, it is necessary to use Fredenhagen–Marcu order parameters [83,84].

V. ADIABATIC STATE PREPARATION AND ANYON BRAIDING

A remarkable property of the Hamiltonian $H_{\mathcal{G}}$ (and $H_{\tilde{\mathcal{G}}}$) [Eq. (2)] is that it can be generalized to *local* transverse fields Ω_s and Ω_l on sites s and links l without violating the local plaquette symmetries $\Theta_p(h)$. The only constraint is that Ω_s (Ω_l) and Δ_s (Δ_l) are equal for all two-level systems that are permuted by these local automorphisms, i.e., transverse fields and detunings must be uniform on each site s and link l, respectively, but can vary between sites and links. This allows us to locally control the system with time-dependent parameters $\Omega_s(t)$ and $\Delta_s(t)$ on sites [$\boldsymbol{\Delta}_s(t)$ for generalized sites], and $\Omega_l(t)$ and $\Delta_l(t)$ on links. In a first step, we leverage this control to propose a protocol for the adiabatic preparation of the flux-free topological quantum many-body ground state of $H_{\mathcal{G}}$. Later, we extend this protocol to realize controlled braiding of flux anyons using $H_{\tilde{\mathcal{G}}}$.

In the following, we restrict the analysis to the regime where the local transverse fields and detunings respect the local symmetries. Starting from a state in the symmetric sector, the system then always remains in this sector. This assumption simplifies the analysis considerably, but is not crucial if the charge gap remains finite (which we expect but cannot prove). We also assume strict blockades ($U_0=\infty$), which simplifies the analysis further; this is also not crucial, as can be shown both numerically and analytically.

A. Adiabatic ground-state preparation

For the adiabatic preparation of the ground state of $H_{\mathcal{G}}$ on a patch of the honeycomb lattice (Fig. 5), we start with $\Omega_i = 0$ and $\Delta_i = -\Delta < 0$ on all vertices, and prepare these two-level systems in the unique ground state $|\psi_0\rangle = \bigotimes_{i\in V}|0\rangle_i$. This state is obviously in the symmetric sector, $|\psi_0\rangle \in \mathcal{H}_{\mathcal{G}}^S$, so that the symmetry sector is completely fixed by this initial state. The main idea for an efficient adiabatic preparation is to *grow* the topological phase, starting from a single site s. On this site, we first adiabatically turn on the transverse field $\Omega_s \sim \Delta$, then ramp the detuning from $\Delta_s = -\Delta < 0$ to its final value $\Delta_s = 4\Delta > 0$, and finally adiabatically turn off the transverse field again, see Fig. 5(a). Because of the strong blockade interaction on the site, only a single vertex can be excited to $|1\rangle$, but since Ω_s acts uniformly on all vertices on s, this protocol results in an equal-weight superposition of all possible single-excitation states,

$$|\psi_1\rangle = \mathcal{N}\left[\bigotimes_{i\notin s}|0\rangle_i\right]\left[\sum_{g_1,g_2\in G}|w_s^{g_1g_2}\rangle\right], \tag{18}$$

with normalization $\mathcal{N} = 1/|G|$. Recall that $|w_s^{g_1g_2}\rangle$ denotes the state with vertex $w_s^{g_1g_2}$ on site s excited to $|1\rangle$ and all other vertices on the site in state $|0\rangle$. During this adiabatic ramping procedure, the system always exhibits a gap of order $\max\{|\Delta_s|, \Omega_s|G|\}$. Note that the transverse field exhibits a collective enhancement because of the blockade interaction, so that for optimal ramping $\Omega_s \sim \Delta/|G|$ and the preparation can be achieved on the time scale $\hbar/\Delta$.

In the next step, we proceed to all links connected to site s and repeat the adiabatic-ramping procedure with $\Omega_l \sim \Delta$ and final value $\Delta_l = 2\Delta$. Because of the blockade interactions between the vertices on the links and the excited vertex on the site, one vertex on each link is in blockade while the others can be efficiently adiabatically excited on the time scale $\hbar/\Delta$. At the end of this procedure, the new ground

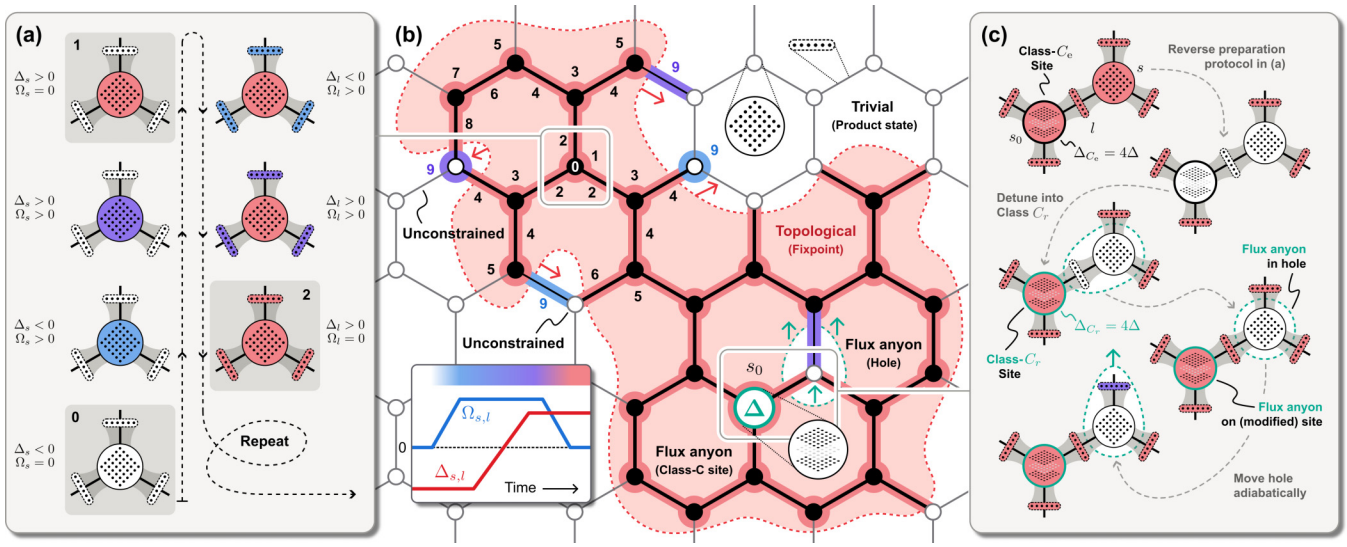

FIG. 5. Adiabatic preparation of ground states and flux anyons. (a), (b) The topological fixed-point ground state can be adiabatically "grown" starting from a completely deexcited array of two-level systems (i.e., $\Delta_s < 0$ and $\Delta_l < 0$ for all sites and links, white filling). One then iterates the ramping procedure (white → blue → purple → red) shown in the inset of (b) for sites and adjacent links repeatedly. Note that transverse fields $\Omega_{s,l}$ and detunings $\Delta_{s,l}$ are adiabatically modified uniformly for all two-level systems on a site or link, thereby respecting the local symmetries of the model at all times. A possible (nonoptimal) initialization sequence is shown in (b) where numbers label time steps. Note that a site (link) can only be initialized in the ground state if there is at least one adjacent link (site) uninitialized (see four cases in time step 9). Since $\Omega_s = 0 = \Omega_l$ after initialization (red area), the prepared ground state is the fixed-point wave function of the quantum double $\tilde{H}_G(0,\omega)$, without admixtures from classical excited states in $\mathcal{H}^{\perp}_{\mathcal{G}}$. (c) Once a patch is prepared in the topological ground state, one can use the generalized site graph $\mathcal{G}_{s_0}[\mathbf{\Delta}]$ to adiabatically inject flux anyons into the system [labeled $\mathbf{\Delta}$ in (b), see Sec. IV for its construction]. The special site s_0 is initialized with $\Delta_{C_e} = -\Delta \nearrow 4\Delta$ (and all other $\Delta_C = -\Delta = \text{const}$) to prepare the no-flux constraint $g_1 g_2 g_3 = \mathrm{e}$. Then this site, together with an adjacent link l and site s, is deexcited again [following the inverse protocol in (a)]. Subsequently, the special site is reinitialized with $\Delta_{C_r} = -\Delta \nearrow 4\Delta$ (green boundary, red filling) so that it enforces the constraint $g_1 g_2 g_3 \in C_r$ for some nontrivial conjugacy class C_r. This protocol prepares two flux anyons in the vacuum fusion channel: $[C_r, E]$ localized on the "flux factory" site s_0, and the corresponding antiparticle $[\bar{C}_r, E]$ in the hole of deexcited sites and links. The hole (carrying its anyon) can then be adiabatically moved by sequences of (de/re)initializations of links and sites (purple link).

state is

$$|\psi_2\rangle = \mathcal{N}\left[\bigotimes_{i\notin s,l} |0\rangle_i\right]\left[\sum_{g_1,g_2\in G} |g_1,g_2,g_3\rangle\big|w_s^{g_1 g_2}\big\rangle\right], \quad (19)$$

where the states $|g_1, g_2, g_3\rangle$ on the three links $l \equiv l_{1,2,3}$ obey the no-flux condition $g_1 g_2 g_3 = \mathrm{e}$ [Fig. 5(a)].

The next step is to repeat the adiabatic ramping on all sites connected to the links l_1, l_2, and l_3, and then proceed with all links connected to these sites, etc. This iterative ramping protocol, alternating between links and sites, grows the topological phase from the inside of the patch toward its boundary, see Fig. 5(b). In each step, the blockade interactions between links and sites constrain the excitation patterns to the ground-state manifold $\mathcal{H}^0_{\mathcal{G}}$. While there is much freedom in the sequence of sites and links that are passed by the ramping procedure [Fig. 5(b)], it is important that for each link only *one* connected site has already been excited, and for each site *at most two* connected links have already been excited. This guarantees that the constraints imposed by the blockade interaction can always be fulfilled. Note that on sites with only *one* connected link already excited, there is still a collectively enhanced coupling $\sqrt{|G|}\Omega_s$, whereas on sites with two excited links there is no collective enhancement. But with proper local addressing, this can be compensated by the strength of the transverse field Ω_s, such that each step can be implemented on a time scale $\sim\hbar/\Delta$.

This protocol prepares a unique state on an open patch of the honeycomb lattice and respects all local symmetries, i.e., the wave function $|\psi_t\rangle$ during the adiabatic ramping always satisfies $\Theta_p(h)|\psi_t\rangle = |\psi_t\rangle$ and remains in the symmetric sector, $|\psi_t\rangle \in \mathcal{H}^S_{\mathcal{G}}$. It is convenient to stop the preparation of a finite patch such that every initialized site has all three emanating links initialized as well, i.e., the patch has "rough" boundaries with dangling links. Then, the protocol prepares the exact and unique ground state of $\tilde{H}_G(0,\omega)$, i.e., the equal-weight superposition of all configurations satisfying the zero-flux constraint on every initialized site. This state corresponds to the unique ground state of the quantum double model (3) for "rough" boundary conditions. Note that after this initialization, it is still possible to ramp up a homogeneous transverse field Ω to prepare the true ground state $|\Omega\rangle$ of the Hamiltonian H_G on a time scale $\sim\hbar/\Delta$ due to the excitation gap in the symmetric sector.

In summary, the adiabatic preparation of the topological state $|\Omega\rangle$ can be achieved on a time scale $\tau \sim 2\sqrt{2A}\,\hbar/\Delta$ with $2A$ the total number of sites in the patch of the honeycomb lattice. As required for the local unitary preparation of a state with topological order from a trivial product state, the time for the preparation scheme scales with the system size (but only with a $\sqrt{A}$ scaling) [79]. Note that if the adiabatic ramping

scheme *violates* the local symmetries, the ramping must be slower than the gap *between* different symmetry sectors to avoid the excitation of charge anyons. In particular, since the charge gap is now essential for the adiabatic preparation, the transverse fields Ω_s and Ω_l can no longer be switched off to prepare the fixed-point ground state. Fortunately, this does not alter the overall scaling of the preparation time with system size.

B. Adiabatic preparation and braiding of flux anyons

The protocol for adiabatic ground-state preparation can be generalized to states with well-defined flux anyons (ground states of $H_{\tilde{\mathcal{G}}}$), and the subsequent adiabatic braiding of these anyons. Flux anyons can be either trapped inside holes, i.e., contiguous areas of sites and links with all vertices in state $|0\rangle$, or pinned to generalized site graphs $\mathcal{G}_s[\mathbf{\Delta}_s]$ (introduced in Sec. IV), where the site-specific chemical potentials $\mathbf{\Delta}_s$ can be used to control the flux anyon type pinned at this site. To prepare well-defined flux anyons with the above method—which is based on the interplay of adiabatic ramping and blockade interactions—one needs at least one special site s_0 with the generalized blockade graph $\mathcal{G}_{s_0}[\mathbf{\Delta}]$, detuned by $\mathbf{\Delta} = \{\Delta_C\}$. This site plays the role of a "flux factory" to adiabatically inject fluxes into the system, which subsequently can be trapped and moved inside holes (which does not require modified sites), see Figs. 5(b) and 5(c). The preparation starts with the initialization of the topological ground state in the symmetric sector $\mathcal{H}^S_{\tilde{\mathcal{G}}}$, with all sites in the zero-flux state. For the generalized site s_0 this means $\Delta_{C_e} = -\Delta \nearrow 4\Delta$ and $\Delta_C = -\Delta = \text{const}$ for all $C \neq C_e$, Fig. 5(c). To inject flux anyons into the system, one selects the special site s_0, an adjacent site s, and the link l connecting them, and applies the inverse adiabatic ramping procedure to bring all vertices on this link and the two sites into state $|0\rangle$. This creates a hole encompassing the two sites, with detunings $\Delta_C = -\Delta$ for all conjugacy classes C on the modified site s_0. To create a flux anyon $[C_r, E]$ and its antiparticle $[\bar{C}_r, E]$ on the two sites, one adiabatically ramps the transverse field Ω_{s_0} on all site vertices, and subsequently the detunings $\Delta_{C_r} = -\Delta \nearrow 4\Delta$ of the site vertices that belong to class C_r (for $C \neq C_r$ the detunings $\Delta_C = -\Delta$ remain constant). Finally, one also performs the ramping on the link to site s. This prepares a state on the three adjacent links that satisfies the generalized condition $g_1 g_2 g_3 \in C_r$. This step creates *two* flux anyons: $[C_r, E]$ pinned at the special site s_0 as the lowest-energy state, and $[\bar{C}_r, E]$ trapped inside the hole at the neighboring site s. Note that the hole necessarily carries the antiflux anyon $[\bar{C}_r, E]$ since the surrounding bulk state requires that these two anyons fuse into the vacuum. Furthermore, the procedure prepares a well-defined state in the fusion space of these two anyons, namely the unique topological state of two anyons $[C_r, E]$ and $[\bar{C}_r, E]$ in the vacuum fusion channel. After this initial creation of a flux pair, the hole can be adiabatically moved around by ramping down a connecting link and an adjacent site, and subsequently ramping up the original site and the connecting link again, Figs. 5(b) and 5(c). In a similar fashion, anyons pinned at site s_0 can first be immersed into a hole and subsequently moved away. Then the "flux factory" s_0 can be reused for the creation of the next pair of flux anyons. Finally, the Wilson loop operators $W^R(\gamma)$ [or $W^C(\gamma)$] for loops γ around flux-carrying holes can be used to measure the enclosed total flux, which probes the fusion channel of the encircled holes.

In summary, we have developed a complete toolbox to explore the non-Abelian character of flux anyons in quantum double models $\mathcal{D}(G)$: (i) adiabatic ground-state preparation, (ii) deterministic and adiabatic creation of flux anyons in a well-defined fusion channel, (iii) adiabatic transport of these anyons (necessary for braiding and fusion), and finally, (iv) probing of fusion channels by measuring Wilson loop operators around flux anyons. In the remainder of this paper, we apply this toolbox to the simplest non-Abelian quantum double $\mathcal{D}(S_3)$.

VI. EXAMPLE: BRAIDING IN $\mathcal{D}(S_3)$

A. Review: The quantum double $\mathcal{D}(S_3)$

For the Abelian group $G = \mathbb{Z}_2$, the construction of the Hamiltonian H_G and its corresponding graph $\mathcal{G}$ reproduces the blockade structure studied in Ref. [61], which leads to an *Abelian* topological phase known as the toric code [5]. Therefore, we focus in the following on the simplest *non-Abelian* quantum double derived from the permutation group $G = S_3 \equiv C_{3v}$ with six elements $\{e, R, R^2, \sigma, \sigma R, \sigma R^2\}$ with R a three-cycle and σ a two-cycle ($\sigma^2 = e$, $R^3 = e$, and $\sigma R = R^2\sigma$). Thus, we have $|G| = N = 6$, so that on each link there are six two-level systems and on each site there are 36 two-level systems; this setup is sketched in Fig. 1(b). The quantum double $\mathcal{D}(S_3)$ features eight anyon types, given by the irreducible representations of the Drinfeld double $\mathcal{D}(S_3)$ [5,67]. In particular, this implies an eightfold ground-state degeneracy on a torus. As discussed in Sec. IV A, the anyons can be labeled by a conjugacy class C of the group G and an irreducible representation of the centralizer of a representative of the conjugacy class. The group S_3 has three conjugacy classes C_e, C_σ, and C_R, and three irreducible representations: the trivial representation E, a one-dimensional representation Γ_1, and a two-dimensional representation Γ_2. Taken together, these label the pure flux anyons and the pure charge anyons. Following the standard notation, these are denoted as $\mathbf{A} \equiv [C_e, E]$ for the vacuum, $\mathbf{D} \equiv [C_\sigma, E]$ and $\mathbf{F} \equiv [C_R, E]$ for the flux anyons, and $\mathbf{B} \equiv [C_e, \Gamma_1]$, and $\mathbf{C} \equiv [C_e, \Gamma_2]$ for the charge anyons. In addition, there are three dyons: $\mathbf{E} \equiv [C_\sigma, \Gamma_\sigma]$ for the nontrivial irreducible representation of the centralizer of C_σ, and $\mathbf{G} \equiv [C_R, \Gamma_{R_1}]$ and $\mathbf{H} \equiv [C_R, \Gamma_{R_2}]$ for the two nontrivial irreducible representations of the centralizer of C_R. A full review of the anyon content of $\mathcal{D}(S_3)$, their fusion channels, F matrices, and R matrices can be found in Ref. [69].

B. Probing the non-Abelian statistics of $\mathcal{D}(S_3)$ with blockade structures

Drawing from the toolbox developed above, we now describe a simple braiding scheme for flux anyons to probe their non-Abelian statistics, see Fig. 6. For this, we start by preparing a setup with four $\mathbf{D} = [C_\sigma, E]$ anyons using (ideally) two "flux factories" as explained in Sec. V B and illustrated in Fig. 6(a). As discussed previously, the initial state is therefore in the fusion channel where the first and second pair of $\mathbf{D}$

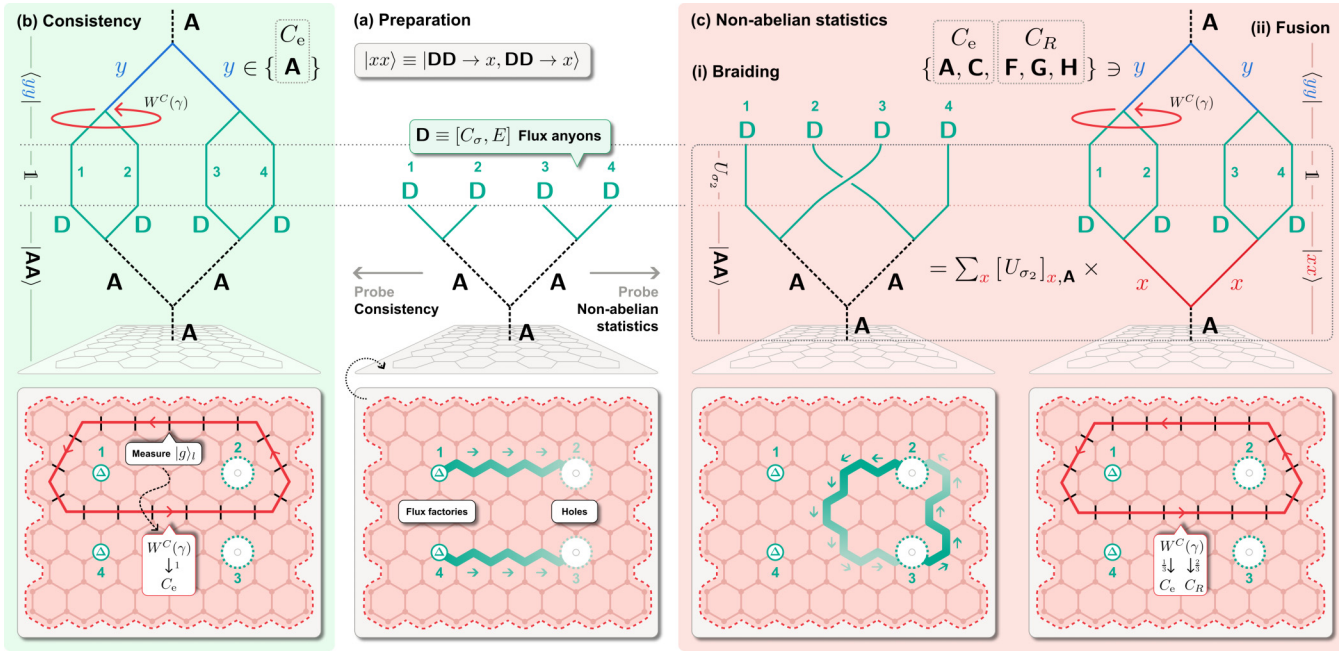

FIG. 6. Probing non-Abelian statistics. Protocol for the preparation, braiding and measurement (fusion) of anyons. The splitting/fusion diagrams (time evolution) are shown in the top row, and the corresponding spatial configurations and manipulations are shown in the bottom row. (a) As an initial step, two pairs (1,2) and (3,4) of $\mathbf{D} = [C_\sigma, E]$ flux anyons (solid green lines) are created and separated within a topological domain (red area) following the protocol described in Sec. V and Fig. 5(c). We denote splitting/fusion states of this form as $|xx\rangle \equiv |\mathbf{DD} \to x, \mathbf{DD} \to x\rangle$. With this nomenclature, the system is initialized in the state $|\mathbf{AA}\rangle$ where both pairs fuse into the vacuum $\mathbf{A}$ (black dashed lines). (b) As a consistency check, the Wilson loop $W^C(\gamma)$ can be computed from measuring the link states $|g\rangle_l$ along the depicted dual loop γ (solid red line). Only for $C = C_\mathrm{e}$ should the expectation value be nonzero since the enclosed anyons are in the vacuum channel. (c) Alternatively, the two anyons 2 and 3 from *different* pairs can be exchanged with a half braid (again using the protocol for adiabatically moving holes) to produce the new state $U_{\sigma_2}|\mathbf{AA}\rangle$ shown in (c)–(i). Here, U_{σ_2} denotes the unitary braiding matrix for exchanging flux 2 and 3. Using the F and R matrices of the unitary braided fusion category that describes the quantum double $\mathcal{D}(S_3)$ (see Appendix C), this state can be expanded in the basis $|xx\rangle$, where the fusion rules allow $x \in \{\mathbf{A}, \mathbf{C}, \mathbf{F}, \mathbf{G}, \mathbf{H}\}$. Here, $\{\mathbf{A}, \mathbf{C}\}$ carry no flux (C_e) and $\{\mathbf{F}, \mathbf{G}, \mathbf{H}\}$ carry nonzero flux of type C_R. These fluxes can be measured again by the same Wilson loop $W^C(\gamma)$, where now the expectation value for $C = C_R$ is finite. This demonstrates the non-Abelian nature of $\mathcal{D}(S_3)$ in that the two states depicted in the lower left and right corners are locally indistinguishable while being linearly independent.

anyons each fuse into the vacuum. It is convenient to define a basis of the fusion space of four $\mathbf{D}$ anyons $\mathcal{H}_\mathbf{A}^\mathbf{DDDD}$ that are in the global vacuum channel $\mathbf{A}$. We denote by $|xx\rangle \equiv |\mathbf{DD} \to x, \mathbf{DD} \to x\rangle$ the fusion state where each pair fuses into anyon x. (Note that both pairs must fuse into the same anyon since the fusion of all four anyons yields the vacuum $\mathbf{A}$ and for $\mathcal{D}(S_3)$ all anyons are their own antiparticle.) The fusion rule [69]

$$\mathbf{D} \otimes \mathbf{D} = \mathbf{A} \oplus \mathbf{C} \oplus \mathbf{F} \oplus \mathbf{G} \oplus \mathbf{H} \tag{20}$$

then determines a basis of the five-dimensional fusion space, namely,

$$\mathcal{H}_\mathbf{A}^\mathbf{DDDD} = \mathrm{span}\,\{|\mathbf{AA}\rangle, |\mathbf{CC}\rangle, |\mathbf{FF}\rangle, |\mathbf{GG}\rangle, |\mathbf{HH}\rangle\}, \tag{21}$$

where our system is initialized in the state $|\mathbf{AA}\rangle$.

Consequently, a measurement of the Wilson loop $W^C(\gamma)$ [via postselection, recall Eq. (17) in Sec. IV C] around the first (and second) pair of anyons must yield the flux C_e with probability 1, which can be used to probe the consistency of the adiabatic preparation scheme, Fig. 6(b). Now we can perform braiding using the adiabatic ramping protocol from Sec. V B, see Fig. 6(c). In general, braiding anyons induces unitary transformations on the fusion space, here $\mathcal{H}_\mathbf{A}^\mathbf{DDDD}$. If we braid the first and second anyon around each other, the fusion state $|\mathbf{AA}\rangle$ remains invariant—which can again be tested by measuring Wilson loop operators. By contrast, if we exchange ("half-braid") the second and the third anyon, the initial state $|\mathbf{AA}\rangle$ transforms into (see Appendix C and Ref. [69])

$$|\mathbf{AA}\rangle \mapsto \frac{1}{3}\Big[\overbrace{|\mathbf{AA}\rangle + \sqrt{2}|\mathbf{CC}\rangle}^{C_\mathrm{e}} + \sqrt{2}\underbrace{\big(|\mathbf{FF}\rangle + e^{i\frac{2\pi}{3}}|\mathbf{GG}\rangle + e^{-i\frac{2\pi}{3}}|\mathbf{HH}\rangle\big)}_{C_R}\Big]. \tag{22}$$

As before, this state can be probed by measuring the Wilson loop around the first two anyons. With probability 1/3 one measures again the trivial flux C_e, but with probability 2/3 one now finds the nontrivial flux C_R. Hence, this simple braiding protocol already reveals the non-Abelian character of the quantum double $\mathcal{D}(S_3)$: by adiabatically exchanging two identical anyons trapped in two holes, one can change

the fusion channel of the system without ever leaving the ground-state manifold.

VII. DISCUSSION AND OUTLOOK

We introduced and studied a family of two-dimensional models, constructed from two-level systems subject to local transverse fields and detunings, where excited states interact via a strong blockade interaction. These models are motivated by the Rydberg platform with neutral atoms in optical tweezers. On an abstract level, the Hamiltonians can be described by vertex-weighted blockade graphs $\mathcal{G}$, with vertices representing two-level systems and edges blockade interactions. We presented a construction for a family of blockade graphs, such that for every finite group G, the ground state of the blockade Hamiltonian with weak transverse fields is in the topologically ordered phase of the quantum double model $\mathcal{D}(G)$. This family of topological phases is characterized by anyonic flux and charge excitations, which exhibit non-Abelian statistics for non-Abelian groups G. We proved the emergence of topological order in the many-body ground state analytically. In an upcoming paper, we show the existence of a finite excitation gap for the special case $G = \mathbb{Z}_2$ [62]. The core idea of our construction is to enforce the no-flux constraint in the ground state by tailored blockade interactions such that the blockade graph exhibits local graph automorphisms. These automorphisms translate to local symmetries of the Hamiltonian, and the symmetric sector corresponds to the zero-charge sector of the corresponding quantum double model. In this framework, we developed a complete toolbox to explore the non-Abelian character of flux anyons. This includes (i) efficient protocols for the adiabatic preparation of ground states, (ii) deterministic and adiabatic preparation schemes for flux anyons in a well-defined fusion channel, (iii) a protocol for the adiabatic transport of these anyons (needed for braiding and fusion), and finally, (iv) a procedure to probe the fusion channel of anyons by measuring Wilson loops around them. Combined, these tools suggest a route for probing non-Abelian topological phases in artificial matter based on realistic two-body interactions.

In this paper, both the construction of the blockade graph $\mathcal{G}$ and the development of the toolbox were illustrated on the trivalent honeycomb lattice as this is the simplest setting to discuss quantum doubles. Note that this is not necessary, and the construction can be straightforwardly generalized to arbitrary lattices and even irregular planar graphs, in accordance with Kitaev's original formulation of quantum doubles [5].

Another generalization concerns the choice of detunings. In our construction of $\mathcal{G}$, the detunings on sites and links were chosen such that $\Delta_s = 2\Delta_l$, combined with a sufficiently large blockade interaction $U_0 > \Delta_s$. These choices are not unique. For example, it is easy to see that the classical ground-state manifold remains unchanged for $\Delta_s > 2\Delta_l$ since larger Δ_s only stabilize the no-flux constraint. An interesting open question is how the phase diagram is affected by variations of these parameters.

While our framework is motivated by the Rydberg platform, we stress that our abstract analysis omits the influence of microscopic van der Waals interactions. To study their effects, a concrete *embedding* of the blockade graphs in two or three dimensions would be necessary. For the special case $G = \mathbb{Z}_2$ (toric code topological order), an explicit embedding of the corresponding blockade graph $\mathcal{G}$ was provided in Ref. [61]. It is an interesting open question whether the proposed blockade graphs for general groups G can be embedded as well, and if so, how to achieve this most efficiently.

Alternatively, the proposed models could be realized on other platforms. Especially cold polar molecules in optical tweezers have recently seen significant progress, with the potential advantage of much longer lifetimes of excited states [63] and a high tunability of interaction potentials [31]. On the other hand, superconducting qubits that are connected by microwave cavities—which act as a bus to mediate blockade interactions [64]—have the potential to realize blockade graphs with fewer restrictions on geometry. Such ideas can naturally be extended to Rydberg atoms in optical cavities that are connected by waveguides. On these platforms, the realization of the blockade graph directly translates to a waveguide structure, and therefore becomes a straightforward engineering task.

We close with a comment on an intriguing though abstract problem. Our construction leads to graphs with local automorphisms that, under certain circumstances, generate a single orbit on the set of maximum-weight independent sets. While there are trivial graphs that satisfy this condition, the maximum-weight independent sets of our models have an intricate structure because of the local constraints; in particular, they cannot be "factorized" (the corresponding low-energy Hilbert space has no local tensor product structure). This raises the question of how graphs with these properties can be classified and/or systematically constructed. This could be useful, as each such graph might give rise to an interesting quantum many-body phase. For example, it would be interesting to explore whether there are graphs that stabilize the topological order of Fibonacci anyons, the simplest anyon model that is universal for topological quantum computation. If this turns out to be *impossible*, it would be helpful to understand *why*, to sharpen our understanding of the limitations of blockade structures.

ACKNOWLEDGMENTS

We thank J.-N. Fuchs for his introduction to quantum double models and S. Michalakis for providing clarifications about the gap stability theorem.

DATA AVAILABILITY

There are no publicly available research data or software supporting this manuscript. Requests for further information or data should be sent to the authors.

APPENDIX A: PROOF OF TOPOLOGICAL ORDER

Here, we provide the detailed proof that the ground state of $H_{\mathcal{G}}$ is topologically ordered for finite $\Omega \neq 0$ (see Sec. III of the main text).

For technical reasons (see Sec. S4 of the SM [74]) we work with periodic boundary conditions. Throughout this section,

we use the following notation: Excitation patterns of two-level systems are described by $\boldsymbol{n} \in \mathbb{Z}_2^n$ with n the number of two-level systems in $\mathcal{G}$. An excitation pattern corresponds to a state $|\boldsymbol{n}\rangle \in \mathcal{H}_\mathcal{G}$; these states form a basis of $\mathcal{H}_\mathcal{G}$. The Hamiltonian $H_\mathcal{G}^0$ is diagonal in this basis. We denote the set of excitation patterns that correspond to ground states of $H_\mathcal{G}^0$ as $\mathcal{L}_\mathcal{G}$. The ground-state manifold is then given by $\mathcal{H}_\mathcal{G}^0 = \text{span}\{\,|\boldsymbol{n}\rangle \,|\, \boldsymbol{n} \in \mathcal{L}_\mathcal{G}\,\}$.

As discussed in Sec. III, the graph $\mathcal{G}$ on a torus is not fully symmetric, i.e., the set of ground-state configurations $\mathcal{L}_\mathcal{G}$ splits into multiple orbits $Q_1, \ldots, Q_O$. Thus, as shown in Ref. [61], the unique ground state for $\Omega \neq 0$ has the form

$$|\Omega\rangle = \sum_{k=1}^{O} \lambda_k(\Omega) \sum_{\boldsymbol{n}\in Q_k} |\boldsymbol{n}\rangle + \sum_{\boldsymbol{n}\notin\mathcal{L}_\mathcal{G}} \eta_{\boldsymbol{n}}(\Omega)|\boldsymbol{n}\rangle. \tag{A1}$$

Note that we have no control over the coefficients $\lambda_k(\Omega)$.

Despite the lack of full symmetry (and the resulting uncontrolled superposition of topological sectors), we can establish that the ground state of $H_\mathcal{G}$ is topologically ordered. To this end, we generalize the technique introduced in Ref. [61]. In this section, we summarize the main argument; technical details for some of the steps are provided in Sec. S4 of the SM [74].

As already stated in Sec. III, we introduce the auxiliary Hamiltonian (11)

$$\tilde{H}_\mathcal{G}(\Omega,\omega) := H_\mathcal{G}(\Omega) + \omega \sum_p \Bigg(\mathbb{1} - \underbrace{\frac{1}{|G|}\sum_h \Theta_p(h)}_{=:\Theta_p}\Bigg). \tag{A2}$$

We say that the term proportional to ω introduces *artificial-plaquette fluctuations*. This term is chosen to resemble the plaquette term of the quantum double Hamiltonian (3). Using this auxiliary Hamiltonian, we can establish topological order in three steps (Fig. 7):

(1) **Step 1: A →B**

At **A** we have $\Omega = \omega = 0$. Thus, the ground-state manifold is extensively degenerate and spanned by the classical ground-state configurations $\mathcal{L}_\mathcal{G}$. The ground-state manifold $\mathcal{H}_\mathcal{G}^0$ is separated by a gap of size $\min_i(\Delta_i)$ from the rest of the spectrum.

To reach **B**, we ramp up the artificial plaquette fluctuations to some value $0 < \omega^* < \Delta$, keeping $\Omega = 0$. As

$$[\tilde{H}_\mathcal{G}(0,\omega^*), \Theta_p] = 0 \quad \text{and} \quad [\Theta_p, \Theta_{p'}] = 0 \tag{A3a}$$

for all plaquettes p, p', the spectrum of $\tilde{H}_\mathcal{G}(0,\omega^*)$ decomposes into sectors labeled by eigenvalues of Θ_p (= symmetry sectors). Since Θ_p is a projector, it has eigenvalues 0 and 1. States with eigenvalue 0 are energetically penalized by the Hamiltonian (A2) with energy ω^*. Thus, the ground states of $\tilde{H}_\mathcal{G}(0,\omega^*)$ are in the sector characterized by $\Theta_p = 1$ for all plaquettes p. The ground-state manifold $\mathcal{H}_\mathcal{G}^{\omega^*}$ of $\tilde{H}_\mathcal{G}(0,\omega^*)$ consists of topologically degenerate ground states that are separated by a gap ω^* from the rest of the spectrum. Moreover, it can be shown (see Sec. S4 A of the SM [74]) that the ground-state manifold can be mapped to the degenerate ground-state manifold $\mathcal{H}_G^{J_p}$ of the quantum double model (3) for $J_p > 0$ by a generalized local unitary transformation. Thus, the Hamiltonians H_G and $\tilde{H}_\mathcal{G}(0,\omega^*)$ describe the same quantum phase; in particular, the states in $\mathcal{H}_\mathcal{G}^{\omega^*}$ are topologically ordered.

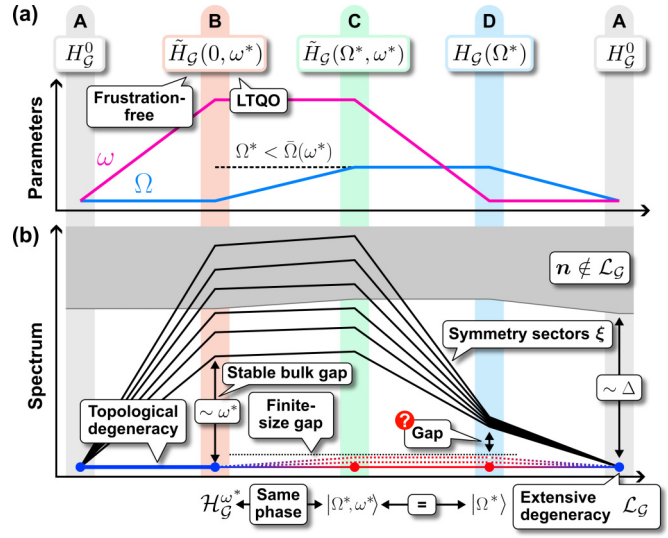

FIG. 7. Proof of topological order. (a) Path that parameterizes the family of Hamiltonians $\tilde{H}_\mathcal{G}(\Omega,\omega)$. Ultimately, we are interested in the quantum phase of the ground state in **D**. Following the path from **A** to **D** allows us to rigorously characterize the quantum phase of the ground state of $H_\mathcal{G}(\Omega)$. (b) Schematic spectrum of $\tilde{H}_\mathcal{G}(\Omega,\omega)$ along the parametric path shown in (a). For $\Omega = \omega = 0$ (**A**), the Hamiltonian $H_\mathcal{G}(0) = \tilde{H}_\mathcal{G}(0,0)$ is classical with an exponentially large, degenerate ground-state manifold $\mathcal{H}_\mathcal{G}^0$ spanned by configurations in $\mathcal{L}_\mathcal{G}$. (**B**) For $\Omega = 0 < \omega^*$, the Hamiltonian $\tilde{H}_\mathcal{G}(0,\omega^*)$ is frustration free and satisfies a condition called *local topological quantum order* (local-TQO). Moreover, its ground-state manifold is separated by a gap of order ω^* from the rest of the spectrum. This ground-state manifold $\mathcal{H}_\mathcal{G}^{\omega^*}$ can be mapped to the ground-state manifold of Kitaev's quantum double model by a generalized local unitary transformation; in particular these states are topologically ordered. Because of frustration freeness and local-TQO, the bulk gap of the Hamiltonian $\tilde{H}_\mathcal{G}(0,\omega^*)$ is stable against weak, local perturbations. Thus, for $\Omega^* < \bar{\Omega}(\omega^*)$, the Hamiltonian $\tilde{H}_\mathcal{G}(\Omega^*,\omega^*)$ (**C**) remains gapped. Here $\bar{\Omega}(\omega^*)$ denotes an upper bound on the perturbation strength that guarantees gap stability. As the gap remains open when ramping up Ω, the new (unique) ground state $|\Omega^*,\omega^*\rangle$ remains topologically ordered. Lastly, switching off $\omega \searrow 0$ leads to the target Hamiltonian $H_\mathcal{G}(\Omega^*) = \tilde{H}_\mathcal{G}(\Omega^*,0)$, the ground state $|\Omega^*\rangle$ of which we want to characterize. Because of the local symmetries, it is $|\Omega^*\rangle = |\Omega^*,\omega^*\rangle$. Note that this construction does not prove the existence of a gap for $H_\mathcal{G}(\Omega^*)$.

(2) **Step 2: B →C**

To reach **C**, we switch on quantum fluctuations with some finite value $\Omega^* \neq 0$. Note that the term $\Omega^* \sum_i \sigma_i^x$ in $H_\mathcal{G}(\Omega^*)$ couples sectors with different excitation numbers. As a consequence, the Hamiltonian $\tilde{H}_\mathcal{G}(\Omega^*,\omega^*)$ can no longer be diagonalized exactly; in particular the ground state changes in an unknown way.

However, as long as the excitation gap above the ground-state manifold does not close when Ω is ramped up, the Hamiltonian $\tilde{H}_\mathcal{G}(\Omega^*,\omega^*)$ describes the same quantum phase as $\tilde{H}_\mathcal{G}(0,\omega^*)$ and consequently also the same quantum phase

as H_G. In particular, it follows that the new (now unique) ground state $|\Omega^*, \omega^*\rangle \in \mathcal{H}_{\mathcal{G}}^{\Omega^*,\omega^*}$ is topologically ordered.

Hence, the remaining problem is to establish gap stability. We remark that this is a priori not obvious, as in general, arbitrarily weak perturbations can close spectral gaps in the thermodynamic limit [76]. Fortunately, the Hamiltonian $\tilde{H}_{\mathcal{G}}(0, \omega^*)$ is *frustration free*, *locally gapped*, and satisfies a condition called *local topological quantum order* (local-TQO). Under these assumptions, it can be shown rigorously that the gap is stable under sufficiently weak, local perturbations [77].

Thus, we can conclude that $|\Omega^*, \omega^*\rangle$ is topologically ordered, as long as $\Omega^* < \bar{\Omega}(\omega^*)$, where $\bar{\Omega}(\omega^*)$ denotes an upper bound on the perturbation strength that guarantees gap stability. For a detailed proof of the gap stability, see Sec. S4 B of the SM [74]. Note that the uniqueness of the ground state $|\Omega^*, \omega^*\rangle$ does not contradict the stability of the phase, since ground-state degeneracies can be lifted by finite-size effects. In particular, Ref. [77] shows that such a splitting of the ground-state degeneracy is exponentially suppressed with increasing system size.

(3) **Step 3: C → D**

In the last step, we switch off the artificial plaquette fluctuations to reach **D** with the desired Hamiltonian $\tilde{H}_{\mathcal{G}}(\Omega^*, 0) = H_{\mathcal{G}}(\Omega^*)$. In contrast to Step 2 above, this change of the Hamiltonian cannot be treated as a small perturbation since $\omega^* \gg \Omega^*$. In addition, $\tilde{H}_{\mathcal{G}}(\Omega^*, \omega^*)$ is *not* frustration free, so the result of Ref. [77] is not applicable. (We are not aware of any gap stability results for frustrated Hamiltonians.)

Now, we utilize the local symmetry projectors Θ_p. By construction, these commute with the full Hamiltonian, i.e., $[\tilde{H}_{\mathcal{G}}(\Omega, \omega), \Theta_p] = 0$. Thus, there exists a basis of eigenstates of both $\tilde{H}_{\mathcal{G}}(\Omega, \omega)$ and Θ_p for all plaquettes p and arbitrary Ω and ω. By Eq. (A2), these states are also eigenstates of $H_{\mathcal{G}}(\Omega)$. Thus, we can label these eigenstates as $|E_\Omega^{\boldsymbol{\xi}}, \boldsymbol{\xi}\rangle$ with

$$H_{\mathcal{G}}(\Omega)\big|E_\Omega^{\boldsymbol{\xi}}, \boldsymbol{\xi}\big\rangle = E_\Omega^{\boldsymbol{\xi}}\big|E_\Omega^{\boldsymbol{\xi}}, \boldsymbol{\xi}\big\rangle, \tag{A4a}$$

$$\Theta_p\big|E_\Omega^{\boldsymbol{\xi}}, \boldsymbol{\xi}\big\rangle = \xi_p\big|E_\Omega^{\boldsymbol{\xi}}, \boldsymbol{\xi}\big\rangle, \tag{A4b}$$

and $\xi_p \in \{0, 1\}$. Equations (A4a) and (A4b) yield an expression for the energy of the states $|E_\Omega^{\boldsymbol{\xi}}, \boldsymbol{\xi}\rangle$,

$$\tilde{H}_{\mathcal{G}}(\Omega, \omega)\big|E_\Omega^{\boldsymbol{\xi}}, \boldsymbol{\xi}\big\rangle = \left[E_\Omega^{\boldsymbol{\xi}} + \omega \sum_p (1 - \xi_p)\right]\big|E_\Omega^{\boldsymbol{\xi}}, \boldsymbol{\xi}\big\rangle. \tag{A5}$$

Consider the ground state $|\Omega^*\rangle$ of $\tilde{H}_{\mathcal{G}}(\Omega^*, 0) = H_{\mathcal{G}}(\Omega^*)$. We cannot directly apply Proposition 1 from Ref. [61] to this Hamiltonian since $\mathcal{G}$ is not necessarily fully symmetric. However, the proof of this proposition shows that $|\Omega^*\rangle$ nevertheless satisfies $\Theta_p(h)|\Omega^*\rangle = |\Omega^*\rangle$ for all $h \in G$ and all plaquettes p. This shows that $\Theta_p|\Omega^*\rangle = |\Omega^*\rangle$ for all plaquettes p, i.e., $|\Omega^*\rangle$ is labeled by $\boldsymbol{\xi} = \mathbf{1}$. Moreover, $|\Omega^*\rangle$ is defined as the eigenvector with the smallest eigenvalue of $H_{\mathcal{G}}(\Omega^*)$. Hence, Eq. (A5) shows that $|\Omega^*\rangle$ is *a* ground state of $\tilde{H}_{\mathcal{G}}(\Omega^*, \omega)$ for all ω.

Let $|E_\Omega^{\boldsymbol{\xi}}, \boldsymbol{\xi}\rangle$ be a ground state of $\tilde{H}_{\mathcal{G}}(\Omega^*, \omega)$. As $|\Omega^*\rangle$ minimizes both terms in Eq. (A5) simultaneously, the same must be true for $|E_\Omega^{\boldsymbol{\xi}}, \boldsymbol{\xi}\rangle$. This implies in particular that $|E_\Omega^{\boldsymbol{\xi}}, \boldsymbol{\xi}\rangle$ is a ground state of $H_{\mathcal{G}}(\Omega^*)$. Since the ground state of $H_{\mathcal{G}}(\Omega^*)$ is unique, it follows that $|E_\Omega^{\boldsymbol{\xi}}, \boldsymbol{\xi}\rangle \propto |\Omega^*\rangle$. Hence, $|\Omega^*\rangle$ is the unique ground state of $\tilde{H}_{\mathcal{G}}(\Omega^*, \omega)$ for all $0 \leqslant \omega \leqslant \omega^*$. This implies in particular that $|\Omega^*, \omega^*\rangle = |\Omega^*\rangle$, hence $|\Omega^*\rangle$ is topologically ordered.

APPENDIX B: WILSON LOOPS

In Sec. IV, we used the Wilson loop (operator) (13) of the quantum double model,

$$\hat{W}^R(\gamma) := \sum_{|\boldsymbol{g}\rangle \in \mathcal{H}_G} \chi_R(g_\gamma)|\boldsymbol{g}\rangle\langle\boldsymbol{g}|, \tag{B1}$$

with product $g_\gamma := \prod_{l\in\gamma} g_l^{\sigma_l}$ along a closed, oriented loop γ on the dual lattice; the sign functions σ_l are defined in Sec. IV (see also Fig. 4). χ_R denotes the character of the irreducible representation (irrep) R of the group G. Note that in Sec. IV we work with the matrix elements of the operator (B1) in the product basis $|\boldsymbol{g}\rangle$ for simplicity.

At the fixed point of the quantum double phase, the measurement of the Wilson-loop operators over all irreps R of the group G uniquely determines the enclosed flux, independent of the shape of the loop. Here, we demonstrate this property by explicitly performing the discrete Fourier transform for class functions,

$$\hat{W}^C(\gamma) := \frac{1}{|Z_G(r_C)|} \sum_R \chi_R^*(r_C)\hat{W}^R(\gamma), \tag{B2}$$

where $Z_G(r_C)$ is the centralizer of the representative $r_C \in C$ of conjugacy class C. Note that $|Z_G(\cdot)|$ is a class function since centralizers of different representatives are isomorphic via conjugation. By the orbit-stabilizer theorem, we can rewrite the cardinality of the centralizer $|Z_G(r_C)| = |G|/|C|$ for any $r_C \in C$; this makes Eqs. (14a) and (B2) equivalent.

The *completeness* of the characters on the set of class functions can be formulated as

$$\sum_R \chi_R^*(g)\chi_R(h) = |Z_G(g)|\delta_{g\sim h}, \tag{B3}$$

where $\delta_{g\sim h} = 1$ if g and h are conjugate and $\delta_{g\sim h} = 0$ otherwise. This allows us to rewrite the Fourier transform (B2) as

$$\hat{W}^C(\gamma) = \sum_{|\boldsymbol{g}\rangle \in \mathcal{H}_G} \delta_{r_C\sim g_\gamma}|\boldsymbol{g}\rangle\langle\boldsymbol{g}|; \tag{B4}$$

where $\delta_{r_C\sim g_\gamma} = 1$ if $g_\gamma \in C$ and $\delta_{r_C\sim g_\gamma} = 0$ otherwise; this shows Eq. (14b).

As an example, consider a state $|C_s\rangle \in \mathcal{H}_{\tilde{\mathcal{G}}}^0 \cap \mathcal{H}_{\tilde{\mathcal{G}}}^S$ where one flux anyon $[C, E]$ is pinned on site s. We consider loops γ that enclose s. Note that the product g_γ is conserved when reshaping the loop over a site without flux anyon (since then $g_1 g_2 g_3 = \mathrm{e}$ for the group elements on the three emanating links). This allows us to contract the loop γ to enclose only the site s with the flux anyon. Then g_γ is just the product of the three group elements of its emanating links, which is in C for all states $|\boldsymbol{g}\rangle$ in the superposition $|C_s\rangle$. Hence, $\langle C_s|\hat{W}^R(\gamma)|C_s\rangle = \chi_R(r_C)$ for some representative $r_C \in C$ (as proposed in Sec. IV) and $\langle C_s|\hat{W}^{C'}(\gamma)|C_s\rangle = \delta_{C',C}$ is nonzero only for $C' = C$.

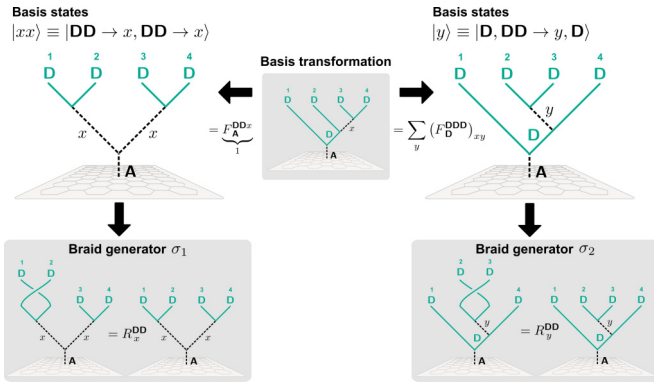

FIG. 8. Basis states and braid group generators. The fusion basis $|xx\rangle \equiv |\mathbf{DD} \to x, \mathbf{DD} \to x\rangle$ of $\mathcal{H}_{\mathbf{A}}^{\mathbf{DDDD}}$, which describes four **D** anyons that fuse into the vacuum **A**, is shown on the left as a splitting diagram. In this basis, the braid generators σ_1 and σ_3 are diagonal with $R_x^{\mathbf{DD}}$. Another basis, $|y\rangle \equiv |\mathbf{D}, \mathbf{DD} \to y, \mathbf{D}\rangle$ is shown on the right. In this basis, the braid generator σ_2 is diagonal with $R_y^{\mathbf{DD}}$. The basis transformation between $|xx\rangle$ and $|y\rangle$ is performed via two F moves: The first is trivial (since $F_{\mathbf{A}}^{\mathbf{DD}x} = 1$) and the second gives rise to a nontrivial basis transformation via $F_{\mathbf{D}}^{\mathbf{DDD}}$.

APPENDIX C: BRAIDING IN $\mathcal{D}(S_3)$

The braid group B_4, which describes the world lines of four anyons that start and end aligned in a row at fixed positions, is generated by three operations: σ_1 exchanges the first anyon with the second, σ_2 the second anyon with the third, and σ_3 the third with the fourth. We define these exchanges with a counterclockwise orientation, as shown in Figs. 6 and 8. In Sec. V, we introduced the basis $|xx\rangle \equiv |\mathbf{DD} \to x, \mathbf{DD} \to x\rangle$ of the fusion space $\mathcal{H}_{\mathbf{A}}^{\mathbf{DDDD}}$, which contains the states with four **D** anyons that fuse into the vacuum **A**. The fusion algebra of $\mathcal{D}(S_3)$ allows for $x \in \{\mathbf{A}, \mathbf{C}, \mathbf{F}, \mathbf{G}, \mathbf{H}\}$, i.e., the first two anyons fuse into x and the remaining two anyons also fuse into x, which finally fuse into the vacuum **A**, see Fig. 8. The fusion outcome of both pairs must be equal because those fuse into the vacuum, and in $\mathcal{D}(S_3)$ all anyons are their own antiparticle. It follows that $\dim \mathcal{H}_{\mathbf{A}}^{\mathbf{DDDD}} = 5$, which reflects the non-Abelian nature of the $\mathcal{D}(S_3)$ anyon theory.

Braiding anyons effects unitary operations on $\mathcal{H}_{\mathbf{A}}^{\mathbf{DDDD}}$. Because of locality, the representations of the two braid generators σ_1 and σ_3 are diagonal in the basis $|xx\rangle$ (braiding two anyons cannot change their fusion channel),

$$\sigma_1 : \ |xx\rangle \mapsto R_x^{\mathbf{DD}} |xx\rangle, \tag{C1a}$$

$$\sigma_3 : \ |xx\rangle \mapsto R_x^{\mathbf{DD}} |xx\rangle, \tag{C1b}$$

with $R_x^{\mathbf{DD}} \in \mathbb{C}$ the R matrices (phases) for braiding two **D** anyons that are in fusion channel x. For the quantum double $\mathcal{D}(S_3)$, one finds [85]

$$R_{\mathbf{A}}^{\mathbf{DD}} = R_{\mathbf{C}}^{\mathbf{DD}} = R_{\mathbf{F}}^{\mathbf{DD}} = 1, \tag{C2a}$$

$$R_{\mathbf{G}}^{\mathbf{DD}} = \bar{\omega}^2, \tag{C2b}$$

$$R_{\mathbf{H}}^{\mathbf{DD}} = \bar{\omega}, \tag{C2c}$$

with $\bar{\omega} = e^{2\pi i/3}$. Note that the last two equations implicitly define which anyons we call **G** and **H**. This was not yet fixed since we did not specify the representations Γ_{R_1} and Γ_{R_2} in Sec. V.

The braid generator that allows us to probe the non-Abelian statistics is σ_2–which is *not* diagonal in the $|xx\rangle$ basis since the fusion channel of anyons 2 and 3 is not determined in this basis. We denote the basis of $\mathcal{H}_{\mathbf{A}}^{\mathbf{DDDD}}$ in which anyons 2 and 3 fuse into $y \in \{\mathbf{A}, \mathbf{C}, \mathbf{F}, \mathbf{G}, \mathbf{H}\}$ as $|y\rangle \equiv |\mathbf{D}, \mathbf{DD} \to y, \mathbf{D}\rangle$. The anyon y then fuses with the fourth **D** anyon into **D**, which finally fuses with the first **D** anyon into the vacuum, see Fig. 8. (The fusion channel of y with the fourth **D** anyon must be **D** because this is the only way to fuse the first **D** anyon into the vacuum **A**.)

Again because of locality, in this basis the unitary representation of the braid generator σ_2 is diagonal,

$$\sigma_2 : \ |y\rangle \mapsto R_y^{\mathbf{DD}} |y\rangle. \tag{C3}$$

The basis change from $|xx\rangle$ to $|y\rangle$ is achieved by two F moves, see Fig. 8, where the first move is trivial because $F_{\mathbf{A}}^{\mathbf{DD}x} = 1$. Consequently, the basis transformation is determined by the matrix $F_{\mathbf{D}}^{\mathbf{DDD}}$,

$$|xx\rangle = \sum_y \left(F_{\mathbf{D}}^{\mathbf{DDD}}\right)_{xy} |y\rangle, \tag{C4}$$

with the F matrix given by [85]

$$F_{\mathbf{D}}^{\mathbf{DDD}} = \frac{1}{3} \begin{pmatrix} 1 & \sqrt{2} & \sqrt{2} & \sqrt{2} & \sqrt{2} \\ \sqrt{2} & 2 & -1 & -1 & -1 \\ \sqrt{2} & -1 & 2 & -1 & -1 \\ \sqrt{2} & -1 & -1 & -1 & 2 \\ \sqrt{2} & -1 & -1 & 2 & -1 \end{pmatrix}. \tag{C5}$$

Here, the order of the basis states is given by $\{\mathbf{A}, \mathbf{C}, \mathbf{F}, \mathbf{G}, \mathbf{H}\}$. Note that $(F_{\mathbf{D}}^{\mathbf{DDD}})^2 = \mathbb{1}$, so that the inverse transformation from basis $|y\rangle$ to $|xx\rangle$ is also given by $F_{\mathbf{D}}^{\mathbf{DDD}}$.

This allows us to express the matrix U_{σ_2}, which represents the braid generator σ_2 in the basis $|xx\rangle$, by first changing to the basis $|y\rangle$, then performing the braid $R_y^{\mathbf{DD}}$, and finally switching back to the basis $|xx\rangle$,

$$U_{\sigma_2} = F_{\mathbf{D}}^{\mathbf{DDD}} \cdot R^{\mathbf{DD}} \cdot F_{\mathbf{D}}^{\mathbf{DDD}} \tag{C6}$$

with the diagonal matrix $(R^{\mathbf{DD}})_{xy} = \delta_{xy} R_y^{\mathbf{DD}}$; this yields [69]

$$U_{\sigma_2} = \frac{1}{3} \begin{pmatrix} 1 & \sqrt{2} & \sqrt{2} & \sqrt{2}\,\bar{\omega} & \sqrt{2}\,\bar{\omega}^2 \\ \sqrt{2} & 2 & -1 & -\bar{\omega} & -\bar{\omega}^2 \\ \sqrt{2} & -1 & 2 & -\bar{\omega} & -\bar{\omega}^2 \\ \sqrt{2}\,\bar{\omega} & -\bar{\omega} & -\bar{\omega} & -\bar{\omega}^2 & 2 \\ \sqrt{2}\,\bar{\omega}^2 & -\bar{\omega}^2 & -\bar{\omega}^2 & 2 & -\bar{\omega} \end{pmatrix}. \tag{C7}$$

Applying this operation to our initial state

$$\langle xx|\mathbf{AA}\rangle = (1 \quad 0 \quad 0 \quad 0 \quad 0)^T \tag{C8}$$

leads to the result in Eq. (22) of the main text.

[1] A. Kitaev and J. Preskill, Topological entanglement entropy, Phys. Rev. Lett. **96**, 110404 (2006).

[2] M. Levin and X.-G. Wen, Detecting topological order in a ground state wave function, Phys. Rev. Lett. **96**, 110405 (2006).

[3] X.-G. Wen, Topological Order: From long-range entangled quantum matter to a unified origin of light and electrons, Int. Scholarly Res. Not. **2013**, 198710 (2013).

[4] X.-G. Wen, Colloquium : Zoo of quantum-topological phases of matter, Rev. Mod. Phys. **89**, 041004 (2017).

[5] A. Kitaev, Fault-tolerant quantum computation by anyons, Ann. Phys. **303**, 2 (2003).

[6] H. Bombin and M. A. Martin-Delgado, Topological quantum distillation, Phys. Rev. Lett. **97**, 180501 (2006).

[7] B. M. Terhal, Quantum error correction for quantum memories, Rev. Mod. Phys. **87**, 307 (2015).

[8] M. H. Freedman, A. Kitaev, M. J. Larsen, and Z. Wang, Topological quantum computation, Bull. Am. Math. Soc. **40**, 31 (2003).

[9] C. Nayak, S. H. Simon, A. Stern, M. Freedman, and S. Das Sarma, Non-Abelian anyons and topological quantum computation, Rev. Mod. Phys. **80**, 1083 (2008).

[10] Z. Wang, Topological Quantum Computation, *Regional Conference Series in Mathematics/Conference Board of the Mathematical Sciences* (American Mathematical Society, Providence, Rhode Island, 2010).

[11] H. Bartolomei, M. Kumar, R. Bisognin, A. Marguerite, J.-M. Berroir, E. Bocquillon, B. Plaçais, A. Cavanna, Q. Dong, U. Gennser, Y. Jin, and G. Fève, Fractional statistics in anyon collisions, Science **368**, 173 (2020).

[12] J. Nakamura, S. Liang, G. C. Gardner, and M. J. Manfra, Direct observation of anyonic braiding statistics, Nat. Phys. **16**, 931 (2020).

[13] K. Pakrouski, M. R. Peterson, T. Jolicoeur, V. W. Scarola, C. Nayak, and M. Troyer, Phase diagram of the $\nu = 5/2$ fractional quantum Hall effect: Effects of Landau-level mixing and nonzero width, Phys. Rev. X **5**, 021004 (2015).

[14] A. Stern, Non-Abelian states of matter, Nature (London) **464**, 187 (2010).

[15] S. C. Zhang, T. H. Hansson, and S. Kivelson, Effective-field-theory model for the fractional quantum Hall effect, Phys. Rev. Lett. **62**, 82 (1989).

[16] A. Lopez and E. Fradkin, Fractional quantum Hall effect and Chern-Simons gauge theories, Phys. Rev. B **44**, 5246 (1991).

[17] B. I. Halperin, P. A. Lee, and N. Read, Theory of the half-filled Landau level, Phys. Rev. B **47**, 7312 (1993).

[18] M. A. Levin and X.-G. Wen, String-net condensation: A physical mechanism for topological phases, Phys. Rev. B **71**, 045110 (2005).

[19] L. Fidkowski, M. Freedman, C. Nayak, K. Walker, and Z. Wang, From string nets to nonabelions, Commun. Math. Phys. **287**, 805 (2009).

[20] A. Kitaev, Anyons in an exactly solved model and beyond, Ann. Phys. **321**, 2, 2 (2006).

[21] N. Lang and H. P. Büchler, Topological states in a microscopic model of interacting fermions, Phys. Rev. B **92**, 041118(R) (2015).

[22] R. M. Lutchyn, J. D. Sau, and S. Das Sarma, Majorana fermions and a topological phase transition in semiconductor-superconductor heterostructures, Phys. Rev. Lett. **105**, 077001 (2010).

[23] L. Fidkowski, R. M. Lutchyn, C. Nayak, and Matthew P. A. Fisher, Majorana zero modes in one-dimensional quantum wires without long-ranged superconducting order, Phys. Rev. B **84**, 195436 (2011).

[24] N. Read and D. Green, Paired states of fermions in two dimensions with breaking of parity and time-reversal symmetries and the fractional quantum Hall effect, Phys. Rev. B **61**, 10267 (2000).

[25] D. A. Ivanov, Non-Abelian statistics of half-quantum vortices in p-Wave superconductors, Phys. Rev. Lett. **86**, 268 (2001).

[26] N. Regnault and B. A. Bernevig, Fractional Chern insulator, Phys. Rev. X **1**, 021014 (2011).

[27] K. Sun, Z. Gu, H. Katsura, and S. Das Sarma, Nearly flatbands with nontrivial topology, Phys. Rev. Lett. **106**, 236803 (2011).

[28] E. Tang, J.-W. Mei, and X.-G. Wen, High-temperature fractional quantum Hall states, Phys. Rev. Lett. **106**, 236802 (2011).

[29] Y. Jia, J. Yu, J. Liu, J. Herzog-Arbeitman, Z. Qi, H. Pi, N. Regnault, H. Weng, B. A. Bernevig, and Q. Wu, Moiré fractional Chern insulators. I. First-principles calculations and continuum models of twisted bilayer $MoTe_2$, Phys. Rev. B **109**, 205121 (2024).

[30] L.-M. Duan, E. Demler, and M. D. Lukin, Controlling spin exchange interactions of ultracold atoms in optical lattices, Phys. Rev. Lett. **91**, 090402 (2003).

[31] A. Micheli, G. K. Brennen, and P. Zoller, A toolbox for lattice-spin models with polar molecules, Nat. Phys. **2**, 341 (2006).

[32] N. C. and, Rapidly rotating atomic gases, Adv. Phys. **57**, 539 (2008).

[33] C. V. Kraus, M. Dalmonte, M. A. Baranov, A. M. Läuchli, and P. Zoller, Majorana edge states in atomic wires coupled by pair hopping, Phys. Rev. Lett. **111**, 173004 (2013).

[34] A. Bühler, N. Lang, C. V. Kraus, G. Möller, S. D. Huber, and H. P. Büchler, Majorana modes and p-wave superfluids for fermionic atoms in optical lattices, Nat. Commun. **5**, 4504 (2014).

[35] N. Y. Yao, A. V. Gorshkov, C. R. Laumann, A. M. Läuchli, J. Ye, and M. D. Lukin, Realizing fractional Chern insulators in dipolar spin systems, Phys. Rev. Lett. **110**, 185302 (2013).

[36] S. Weber, R. Bai, N. Makki, J. Mögerle, T. Lahaye, A. Browaeys, M. Daghofer, N. Lang, and H. P. Büchler, Experimentally accessible scheme for a fractional Chern insulator in Rydberg atoms, PRX Quantum **3**, 030302 (2022).

[37] C. Chamon, D. Green, and Z.-C. Yang, Constructing quantum spin liquids using combinatorial gauge symmetry, Phys. Rev. Lett. **125**, 067203 (2020).

[38] Z.-C. Yang, D. Green, H. Yu, and C. Chamon, $\mathbb{Z}_3$ Quantum Double in a Superconducting Wire Array, PRX Quantum **2**, 030327 (2021).

[39] D. Green and C. Chamon, Constructing non-Abelian quantum spin liquids using combinatorial gauge symmetry, SciPost Phys. **15**, 067 (2023).

[40] H. Yu, D. Green, A. E. Ruckenstein, and C. Chamon, Abelian combinatorial gauge symmetry, SciPost Phys. Core **7**, 014 (2024).

[41] H. Yu, D. Green, and C. Chamon, Non-Abelian combinatorial gauge theory, Phys. Rev. B **111**, 235115 (2025).

[42] S. de Léséleuc, V. Lienhard, P. Scholl, D. Barredo, S. Weber, N. Lang, H. P. Büchler, T. Lahaye, and A. Browaeys, Observation of a symmetry-protected topological phase of interacting bosons with Rydberg atoms, Science **365**, 775 (2019).

[43] R. Verresen, M. D. Lukin, and A. Vishwanath, Prediction of toric code topological order from Rydberg blockade, Phys. Rev. X **11**, 031005 (2021).

[44] G. Semeghini, H. Levine, A. Keesling, S. Ebadi, T. T. Wang, D. Bluvstein, R. Verresen, H. Pichler, M. Kalinowski, R. Samajdar, A. Omran, S. Sachdev, *et al.*, Probing topological spin liquids on a programmable quantum simulator, Science **374**, 1242 (2021).

[45] R. Sahay, A. Vishwanath, and R. Verresen, Quantum spin puddles and lakes: NISQ-era spin liquids from non-equilibrium dynamics, arXiv:2211.01381.

[46] G. Giudici, M. D. Lukin, and H. Pichler, Dynamical preparation of quantum spin liquids in Rydberg atom arrays, Phys. Rev. Lett. **129**, 090401 (2022).

[47] F. Nogrette, H. Labuhn, S. Ravets, D. Barredo, L. Béguin, A. Vernier, T. Lahaye, and A. Browaeys, Single-atom trapping in holographic 2D arrays of microtraps with arbitrary geometries, Phys. Rev. X **4**, 021034 (2014).

[48] D. Barredo, S. de Léséleuc, V. Lienhard, T. Lahaye, and A. Browaeys, An atom-by-atom assembler of defect-free arbitrary two-dimensional atomic arrays, Science **354**, 1021 (2016).

[49] H. Bernien, S. Schwartz, A. Keesling, H. Levine, A. Omran, H. Pichler, S. Choi, A. S. Zibrov, M. Endres, M. Greiner, V. Vuletić, and M. D. Lukin, Probing many-body dynamics on a 51-atom quantum simulator, Nature (London) **551**, 579 (2017).

[50] D. Barredo, V. Lienhard, S. de Léséleuc, T. Lahaye, and A. Browaeys, Synthetic three-dimensional atomic structures assembled atom by atom, Nature (London) **561**, 79 (2018).

[51] D. Jaksch, J. I. Cirac, P. Zoller, S. L. Rolston, R. Côté, and M. D. Lukin, Fast quantum gates for neutral atoms, Phys. Rev. Lett. **85**, 2208 (2000).

[52] M. Saffman, T. G. Walker, and K. Mølmer, Quantum information with Rydberg atoms, Rev. Mod. Phys. **82**, 2313 (2010).

[53] D. Barredo, H. Labuhn, S. Ravets, T. Lahaye, A. Browaeys, and C. S. Adams, Coherent excitation transfer in a spin chain of three Rydberg atoms, Phys. Rev. Lett. **114**, 113002 (2015).

[54] H. Pichler, S.-T. Wang, L. Zhou, S. Choi, and M. D. Lukin, Computational complexity of the Rydberg blockade in two dimensions, arXiv:1809.04954.

[55] C. J. Turner, A. A. Michailidis, D. A. Abanin, M. Serbyn, and Z. Papić, Weak ergodicity breaking from quantum many-body scars, Nat. Phys. **14**, 745 (2018).

[56] C.-J. Lin and O. I. Motrunich, Exact quantum many-body scar states in the Rydberg-blockaded atom chain, Phys. Rev. Lett. **122**, 173401 (2019).

[57] D. Bluvstein, A. Omran, H. Levine, A. Keesling, G. Semeghini, S. Ebadi, T. T. Wang, A. A. Michailidis, N. Maskara, W. W. Ho, S. Choi, M. Serbyn, *et al.*, Controlling quantum many-body dynamics in driven Rydberg atom arrays, Science **371**, 1355 (2021).

[58] S. Ebadi, A. Keesling, M. Cain, T. T. Wang, H. Levine, D. Bluvstein, G. Semeghini, A. Omran, J.-G. Liu, R. Samajdar, X.-Z. Luo, B. Nash, *et al.*, Quantum optimization of maximum independent set using Rydberg atom arrays, Science **376**, 1209 (2022).

[59] M.-T. Nguyen, J.-G. Liu, J. Wurtz, M. D. Lukin, S.-T. Wang, and H. Pichler, Quantum optimization with arbitrary connectivity using Rydberg atom arrays, PRX Quantum **4**, 010316 (2023).

[60] S. Stastny, H. P. Büchler, and N. Lang, Functional completeness of planar Rydberg blockade structures, Phys. Rev. B **108**, 085138 (2023).

[61] T. F. Maier, H. P. Büchler, and N. Lang, Topological order in symmetric blockade structures, PRX Quantum **6**, 030340 (2025).

[62] S. Fell, T. F. Maier, H. P. Büchler, and N. Lang (unpublished).

[63] D. K. Ruttley, T. R. Hepworth, A. Guttridge, and S. L. Cornish, Long-lived entanglement of molecules in magic-wavelength optical tweezers, Nature (London) **637**, 827 (2025).

[64] A. Blais, A. L. Grimsmo, S. M. Girvin, and A. Wallraff, Circuit quantum electrodynamics, Rev. Mod. Phys. **93**, 025005 (2021).

[65] R. M. Karp, *Reducibility Among Combinatorial Problems* (Springer, Berlin, 2009), pp. 219–241.

[66] B. N. Clark, C. J. Colbourn, and D. S. Johnson, Unit disk graphs, Discrete Math. **86**, 165 (1990).

[67] S. H. Simon, *Topological Quantum* (Oxford University Press, Oxford, 2023).

[68] H. Bombin and M. A. Martin-Delgado, Family of non-Abelian Kitaev models on a lattice: Topological condensation and confinement, Phys. Rev. B **78**, 115421 (2008).

[69] S. X. Cui, S.-M. Hong, and Z. Wang, Universal quantum computation with weakly integral anyons, Quant. Info. Proc. **14**, 2687 (2015).

[70] A. Kómár and O. Landon-Cardinal, Anyons are not energy eigenspaces of quantum double Hamiltonians, Phys. Rev. B **96**, 195150 (2017).

[71] S. X. Cui, D. Ding, X. Han, G. Penington, D. Ranard, B. C. Rayhaun, and Z. Shangnan, Kitaev's quantum double model as an error correcting code, Quantum **4**, 331 (2020).

[72] R. Dijkgraaf, V. Pasquier, and P. Roche, Quasi Hopf algebras, group cohomology and orbifold models, Nucl. Phys. B Proc. Suppl. **18**, 60 (1991).

[73] S. Majid, Quantum double for quasi-Hopf algebras, Lett. Math. Phys. **45**, 1 (1998).

[74] See Supplemental Material at http://link.aps.org/supplemental/10.1103/99sy-kggw for details on the construction of the blockade graphs, their automorphism group, and on the proof of ground state topological order.

[75] On a torus, not all ground state configurations $|\boldsymbol{g}\rangle \in \mathcal{H}^0_{\mathcal{G}}$ (satisfying the no-flux constraint on every site) can be generated by applying plaquette (or loop) automorphisms on the state $|\mathbf{e}\rangle$ with all $g_l = \mathrm{e}$. This partitions $\mathcal{H}^0_{\mathcal{G}}$ into topological sectors, and the amplitudes in the (unique) ground state between these sectors are not necessarily fixed by symmetries.

[76] S. Bravyi, M. B. Hastings, and S. Michalakis, Topological quantum order: Stability under local perturbations, J. Math. Phys. **51**, 093512 (2010).

[77] S. Michalakis and J. P. Zwolak, Stability of frustration-free Hamiltonians, Commun. Math. Phys. **322**, 277 (2013).

[78] S. Bravyi and M. B. Hastings, A short proof of stability of topological order under local perturbations, Commun. Math. Phys. **307**, 609 (2011).

[79] X. Chen, Z.-C. Gu, and X.-G. Wen, Local unitary transformation, long-range quantum entanglement, wave function renormalization, and topological order, Phys. Rev. B **82**, 155138 (2010).

[80] S. Bravyi, D. P. DiVincenzo, and D. Loss, Schrieffer-Wolff transformation for quantum many-body systems, Ann. Phys. **326**, 2793 (2011).

[81] V. G. Drinfel'd, Quantum groups, J. Sov. Math. **41**, 898 (1988).

[82] K. G. Wilson, Confinement of quarks, Phys. Rev. D **10**, 2445 (1974).

[83] K. Fredenhagen and M. Marcu, Charged states in $\mathbb{Z}_2$ gauge theories, Commun. Math. Phys. **92**, 81 (1983).

[84] K. Gregor, D. A. Huse, R. Moessner, and S. L. Sondhi, Diagnosing deconfinement and topological order, New J. Phys. **13**, 025009 (2011).

[85] The Sage Developers, sagemath, the Sage mathematics software system, Zenodo, 2026, https://doi.org/10.5281/zenodo.14600115.